

Article

Interval Type-II Fuzzy Fault-Tolerant Control for Constrained Uncertain 2-DOF Robotic Multi-Agent Systems with Active Fault Detection

Wen Yan , Haiyan Tu , Peng Qin and Tao Zhao

College of Electrical Engineering, Sichuan University, Chengdu 610065, China; yanwenessay@stu.scu.edu.cn (W.Y.); qinpeng1@stu.scu.edu.cn (P.Q.); zhaotaozhaogang@scu.edu.cn (T.Z.)

* Correspondence: haiyant@scu.edu.cn

Abstract: This study proposed a novel adaptive interval Type-II fuzzy fault-tolerant control for constrained uncertain 2-DOF robotic multi-agent systems with an active fault-detection algorithm. This control method can realize the predefined-accuracy stability of multi-agent systems under input saturation constraint, complex actuator failure and high-order uncertainties. Firstly, a novel active fault-detection algorithm based on pulse-wave function was proposed to detect the failure time of multi-agent systems. To the best of our knowledge, this was the first time that an active fault-detection strategy had been used in multi-agent systems. Then, a switching strategy based on active fault detection was presented to design the active fault-tolerant control algorithm of the multi-agent system. In the end, based on the interval type-II fuzzy approximated system, a novel adaptive fuzzy fault-tolerant controller was proposed for multi-agent systems to deal with system uncertainties and redundant control inputs. Compared with other relevant fault-detection and fault-tolerant control methods, the proposed method can achieve predefinition of stable accuracy with smoother control input. The theoretical result was verified by simulation.

Keywords: active fault detection; adaptive fuzzy fault-tolerant control; multi-agent systems



Citation: Yan, W.; Tu, H.; Qin, P.; Zhao, T. Interval Type-II Fuzzy Fault-Tolerant Control for Constrained Uncertain 2-DOF Robotic Multi-Agent Systems with Active Fault Detection. *Sensors* **2023**, *23*, 4836. <https://doi.org/10.3390/s23104836>

Academic Editors: Wu Deng and Huimin Zhao

Received: 7 April 2023
Revised: 6 May 2023
Accepted: 10 May 2023
Published: 17 May 2023



Copyright: © 2023 by the authors. Licensee MDPI, Basel, Switzerland. This article is an open access article distributed under the terms and conditions of the Creative Commons Attribution (CC BY) license (<https://creativecommons.org/licenses/by/4.0/>).

1. Introduction

In recent years, multi-agent systems have been widely used in robots, factories, laboratories and networks [1–4]. However, because of actuator failure and system uncertainty, intelligent fault-tolerant control of multiple agents has become a research hotspot [5,6].

The existing fault-tolerant control strategies are mainly divided into passive fault-tolerant control strategies and active ones [7–9]. Most passive fault-tolerant control methods are based on robust control strategy, but this control strategy is often conservative and requires prior fault information [7]. In order to solve the defect that the fault information in passive fault-tolerant control needs prior information, the active fault-tolerant control was proposed by adding a fault-detection and diagnosis module [10]. This strategy can realize the online reconstruction of the controller without prior fault information. An active fault-tolerant control method was proposed by integrating detection, diagnosis and controller reconstruction, but it may be unstable in the detection and diagnosis stages [11]. In order to solve this stability problem, an active fault-tolerant control method was proposed as a robust control idea to deal with the conflict between stabilization and restructuring [12]. After that, active fault-tolerant control has been widely used in various mechanical control systems. Active fault-tolerant control was applied to unmanned aerial vehicles (UAVs), which achieved the rapid stability of the control system under actuator failure [13]. In order to solve the stability problem of underwater robots under actuator fault conditions, an active fault-tolerant control was used to realize the stability of the closed-loop system [14,15]. In order to improve the fault-tolerant control performance of the manipulator, an active fault-tolerant control based on redundant motors was proposed to reduce the structural

complexity [16]. In order to improve the performance of fault-tolerant controls under noisy conditions, fault detection was often used [17–21]. With the development of fault-detection technology, it was applied in many fields [22–26]. However, traditional active fault-tolerant controls mainly relied on a passive detection mechanism. In systems with complex uncertainties and faults, the passive detection mechanism may not be sensitive enough to detect faults. In order to improve the sensitivity of the detection stage, an active fault-detection algorithm was proposed by adding auxiliary input signals [27]. Since the active fault-detection algorithm can identify more complex and variable faults, it has been studied by some scholars [28–30]. However, the existing active detection algorithms are mainly for single-agent systems and few are for multi-agent systems. The subsystem faults of multi-agent systems are often different and the sensors are interfered with by multiple subsystems. As a result, the detection mechanism may be insensitive to faults and thus trigger incorrectly. Furthermore, the constraints of multi-agent controllers are also very complex [31] and the control input saturation is not considered in most fault-tolerant control methods for multi-agent systems. Hence, it is a challenge to detect complex faults in multi-agent systems.

The actual control system often contains complex and changeable uncertainties, and fuzzy logic systems are often used to approximate system uncertainty because of their good approximation performance [32–35]. It is often difficult to deal with high-order uncertainties with traditional fuzzy logic systems, so type-II fuzzy control was proposed to improve the approximation performance to complex uncertainties [36]. The calculation of traditional Type-II fuzzy logic systems is often slow, so an interval Type-II fuzzy logic system was applied to the design of the controller [37]. In order to make the fuzzy logic system approximate the rapidly changing uncertainty, an adaptive fuzzy control strategy was proposed based on the adaptive adjustment of weight parameters [38]. Based on that, the weight adaptive law was applied to interval Type-II fuzzy control to deal with high-order uncertainties and changeable uncertainties [39]. By considering the fault-tolerant control algorithm, an interval Type-II fuzzy fault-tolerant control was proposed to deal with system faults and system uncertainties at the same time [40]. However, most existing interval Type-II fuzzy fault-tolerant control methods are based on passive fault detection [40–42]. This passive detection has difficulty distinguishing between faults and the uncertainty of multi-agent systems, which is caused by the strong coupling of multiple subsystems. This problem may make it difficult for the fuzzy system to approximate the actual uncertainty and affect the system control performance. Meanwhile, the active fault-tolerant control strategy of the multi-agent system can also lead to fast changes in uncertainty. Therefore, it is valuable to study adaptive interval Type-II fuzzy fault-tolerant controls for multi-agent systems.

Motivated by the above-mentioned problem, we propose a novel adaptive interval Type-II fuzzy fault-tolerant control for the proposed multi-agent systems based on active fault detection. This control method can realize the predefined-accuracy stability of multi-agent systems under input saturation, complex actuator failure and high-order uncertainties. The main innovative contributions are listed in the following:

- (1) To the best of our knowledge, active fault detection of multi-agent systems is realized for the first time. Compared with the existing passive fault-detection methods, the novel active detection algorithm can resist more topology communication interference than passive detection.
- (2) An improved fault-tolerant control algorithm of multi-agent systems was designed by the novel active fault-detection switching strategy. Compared with the existing passive fault-tolerant control methods, the proposed method can handle more serious and complex actuator failures in multi-agent systems.
- (3) Based on the interval Type-II fuzzy approximated system, a novel adaptive fuzzy fault-tolerant controller was proposed for multi-agent systems to deal with high-order uncertainties and redundant control inputs. Compared with other fault-tolerant control methods, the proposed method can achieve predefinition of stable accuracy.

In the following, Section 2 presents the preliminaries. Section 3 is the problem description. Section 4 presents the results. Section 5 is the simulation analysis. Section 6 is the conclusion.

2. Preliminaries

Assumption 1 ([43–45]). Assume that only the failures given in Definition 2 occur during system operation and no additional failures occur. The soundness of the system can be ensured in this study.

Lemma 1 ([32]). Consider a continuous function: $f(\mathbf{x}) : D_f \rightarrow \mathbb{R}$ and D_f is the compact set. Then, $f(\mathbf{x})$ can be approximated by an interval Type-II fuzzy logic system $\hat{\mathbf{w}}^T \boldsymbol{\beta}(\mathbf{x})$ with arbitrary small error δ :

$$|f(\mathbf{x}) - \hat{\mathbf{w}}^T \boldsymbol{\beta}(\mathbf{x})| \leq \delta \quad (1)$$

where $\hat{\mathbf{w}} \in \mathbb{R}^r$ is the adaptive weight parameter vector. $\hat{\mathbf{w}} \in \mathbb{R}^r$ is the expected weight parameter vector. $\boldsymbol{\beta}(\mathbf{x}) \in \mathbb{R}^{\prod_{i=1}^n r_i}$ is a basis function as shown in Figure 1, which can be expressed as:

$$\beta_r(\mathbf{x}) = \beta_r^L(\mathbf{x})\vartheta_r + \beta_r^U(\mathbf{x})\bar{\vartheta}_r \quad (2)$$

in which

$$\begin{aligned} \beta_r^{LU}(\mathbf{x}) &= \left[\prod_{\phi}^{h=1} \mu_{\tilde{A}_h^L}^L(\mathbf{x}), \prod_{\phi}^{h=1} \mu_{\tilde{A}_h^U}^U(\mathbf{x}) \right] \\ &= [\beta_r^L(\mathbf{x}), \beta_r^U(\mathbf{x})] \end{aligned} \quad (3)$$

here, $\vartheta_r + \bar{\vartheta}_r = 1$. $\mu_{\tilde{A}_h^L}^L(\mathbf{x})$ and $\mu_{\tilde{A}_h^U}^U(\mathbf{x})$ are the lower and upper membership grades:

$$\begin{cases} \mu_{\tilde{A}_h^L}^L(x_h) = \exp\left(-\frac{1}{2}\left(\frac{x_h - m_{h,r}^L}{\sigma_h^L}\right)^2\right) \\ \mu_{\tilde{A}_h^U}^U(x_h) = \exp\left(-\frac{1}{2}\left(\frac{x_h - m_{h,r}^U}{\sigma_h^U}\right)^2\right) \end{cases} \quad (4)$$

with the following fuzzy rules:

$$\begin{aligned} \text{Rule}^r : & \text{ IF } x_1 \text{ is } \tilde{A}_1^r \text{ and } \dots \text{ and } x_n \text{ is } \tilde{A}_n^r, \\ & \text{ Then } \hat{\mathbf{w}}^T \boldsymbol{\beta}(\mathbf{x}) \text{ is } \tilde{B}^r \end{aligned} \quad (5)$$

Here, the fuzzy set is considered as the complete and continuous set [46–51].

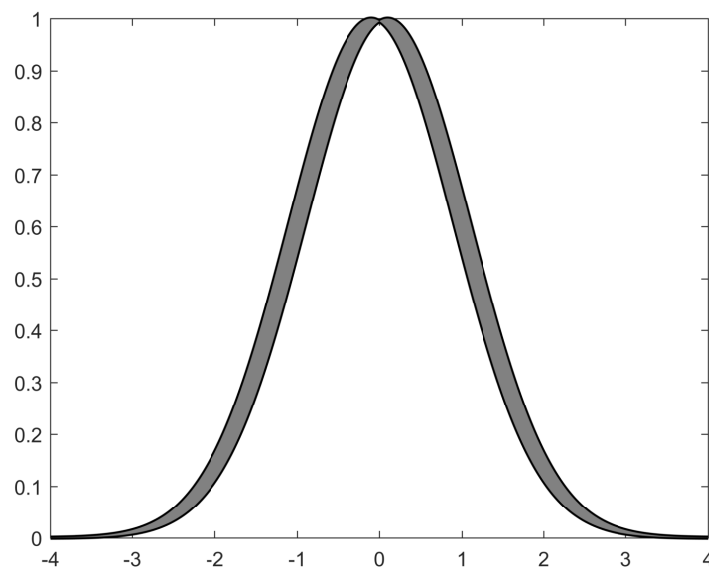


Figure 1. Interval Type-II fuzzy membership function.

3. Problem Description

Multi-agent systems are based on graph theory and the relevant background is described in Appendix A.

Definition 1. A 2-DOF robotic multi-agent system is defined with a leader and N ($N \geq 2$) followers:

$$\begin{cases} \dot{\mathbf{q}}_{i,1} = \mathbf{q}_{i,2} \\ \dot{\mathbf{q}}_{i,2} = \mathbf{f}_i(\mathbf{q}_{i,1}, \mathbf{q}_{i,2}) + \Delta \mathbf{f}_i(\mathbf{q}_{i,1}, \mathbf{q}_{i,2}) + (\mathbf{g}_i(\mathbf{q}_{i,1}) + \Delta \mathbf{g}_i(\mathbf{q}_{i,1}))(\mathbf{u}_i + \mathbf{u}_{a_i}) \end{cases} \quad (6)$$

and the dynamic model of the leader is described as follows ($i = l$):

$$\begin{cases} \dot{\mathbf{q}}_{l,1} = \mathbf{q}_{l,2} \\ \dot{\mathbf{q}}_{l,2} = \mathbf{f}_l(\mathbf{q}_{l,1}, \mathbf{q}_{l,2}) + \Delta \mathbf{f}_l(\mathbf{q}_{l,1}, \mathbf{q}_{l,2}) + (\mathbf{g}_l(\mathbf{q}_{l,1}) + \Delta \mathbf{g}_l(\mathbf{q}_{l,1}))(\mathbf{u}_l + \mathbf{u}_{a_l}) \end{cases} \quad (7)$$

where $\mathbf{q}_{i,1} = [q_{i,1,1}, \dots, q_{i,1,n}]^T$ and $\mathbf{q}_{i,2} = [q_{i,2,1}, \dots, q_{i,2,n}]^T$. $\mathbf{u}_i = [u_{i,1}, \dots, u_{i,n}]^T$ represents the main control input and \mathbf{u}_{a_i} represents the redundant control input. $\mathbf{f}_i(\mathbf{q}_{i,1}, \mathbf{q}_{i,2}) = -\mathbf{M}_i(\mathbf{q}_{i,1})^{-1}(\mathbf{C}_i(\mathbf{q}_{i,1}, \mathbf{q}_{i,2})\mathbf{q}_{i,2} + \mathbf{G}_i(\mathbf{q}_{i,1}))$, in which $\mathbf{M}_i(\mathbf{q}_{i,1})$ is the symmetric inertia matrix, $\mathbf{C}_i(\mathbf{q}_{i,1}, \mathbf{q}_{i,2})$ is the centripetal and Coriolis torques matrix and $\mathbf{G}_i(\mathbf{q}_{i,1})$ is the gravitational torque. $\mathbf{g}_i(\mathbf{q}_{i,1}) = \mathbf{M}_i(\mathbf{q}_{i,1})^{-1}$. $\Delta \mathbf{f}_i(\mathbf{q}_{i,1}, \mathbf{q}_{i,2})$ and $\Delta \mathbf{g}_i(\mathbf{q}_{i,1})$ denote the unknown uncertainties caused by parameter perturbation and modeling uncertainty. When the subscript i is replaced by l , the symbolic meaning is that of the leader. Uncertainty from multiple sources can be called high-order uncertainty.

The tracking error of i th follower in (6) is defined as:

$$\mathbf{z}_{i,1} = \sum_{h=1}^N a_{ih}(\mathbf{q}_{i,1} - \mathbf{q}_{h,1}) + b_i(\mathbf{q}_{i,1} - \mathbf{q}_{l,1}) \quad (8)$$

where a_{ih} and b_i are the weight parameters.

Condition 1. The input constraint is $|u_{i,k}| \leq U$, in which U is the known and bounded constant.

Lemma 2. In order to achieve Condition 1, the actual control input $u_{i,k}$ can be designed by [52] as:

$$u_{i,k} = U \tanh\left(\frac{v_{i,k}}{U}\right) \quad (9)$$

where $v_{i,k} = u_{i,k}(v_{i,k}) + e(v_{i,k})$. $e_{i,k}(v_{i,k}) \leq E$ and E is a bounded unknown constant.

Definition 2. The faults of sub-systems for multi-agent systems are often various, so their overall fault situation is complex. The actuator fault of subsystem [5] is considered as the following:

$$u_{f_{i,k}} = \Psi_{i,k}(q_{i,1,k}, t)u_{i,k} + \Phi_{i,k}(t) \quad (10)$$

in which

$$\Psi_{i,k}(q_{i,1,k}, t) = \begin{cases} \exp(-\eta_{i,k}t + \omega_{i,k}) + 0.1\sin(q_{i,1,k}), & t \geq t_{a_{i,k}} \\ 1, & t < t_{a_{i,k}} \end{cases} \quad (11)$$

where $\eta_{i,k}t_{act} = \omega_{i,k}$. $\eta_{i,k}$ and $\omega_{i,k}$ are the positive parameters. $t_{a_{i,k}}$ is the failure time of actuator. $\Phi_{i,k}(t)$ is considered to be zero in this paper.

The control objective is to make the tracking error of the system converge to the predefined accuracy \dagger before and after the fault occurs.

4. Results

The design scheme of the proposed controller is shown in Figure 2. Assumption 1 is satisfied and the system is considered optimized [53–57].

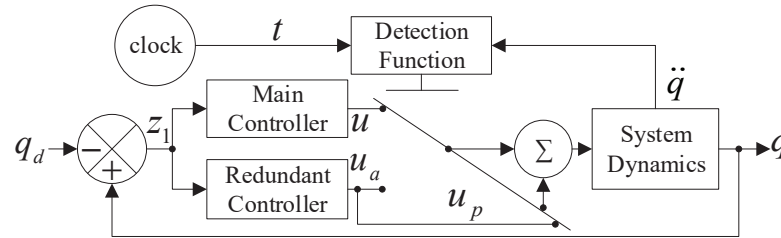


Figure 2. The controller structure block diagram of the agent.

4.1. Active Fault Detection and Fault-Tolerant Control

The auxiliary input signal of redundant controller u_p is considered as a pulse-wave function:

$$u_p(t) = \begin{cases} \mathbf{U}_m, & \kappa t_p + t_0 \leq t \leq \kappa t_p + t_0 + \Delta t \\ 0, & \text{others} \end{cases} \quad (12)$$

where $\kappa = 1, 2, 3, \dots$. $\mathbf{U}_m = [U_m, \dots, U_m]^T$ is the pulse amplitude vector. t_p is the pulse repetition period. t_0 is the start time of detection. Δt is the pulse width.

By observing (6) and (7), it is clear that observable information $\dot{q}_{i,2}$ is more sensitive to the change of control input u_{a_i} than other observable information $q_{i,2}$ and $q_{i,1}$. Hence, a novel active detection algorithm is designed as follows.

When $flag = 1$ in Algorithm 1, the system is judged to be faulty. Then, the following improved active fault-tolerant control algorithm is activated:

Algorithm 1 Active fault-detection algorithm ($i = l, 1, 2, 3, \dots$)

Initial stage

$$u_i = U \tanh\left(\frac{z_i}{U}\right)$$

$$u_{a_i} = u_{p_i}$$

Initial Y (A fault threshold parameter)

Global Flag

The 1th detection cycle(2)

$$\text{If } t \approx t_p + t_0 + \Delta t$$

$$\text{If } \|\dot{q}_{i,2}(t) - \dot{q}_{i,2}(t - \Delta t)\| > \|\dot{q}_{i,2}(t - t_1) - \dot{q}_{i,2}(t - t_1 - \Delta t)\| + Y$$

$$Flag = 1$$

end

end

⋮

The $\kappa - 1$ th detection cycle(κ)

$$\text{If } t \approx \kappa t_p + t_0 + \Delta t$$

$$\text{If } \|\dot{q}_{i,2}(t) - \dot{q}_{i,2}(t - \Delta t)\| > \|\dot{q}_{i,2}(t - t_p) - \dot{q}_{i,2}(t - t_p - \Delta t)\| + Y$$

$$Flag = 1$$

end

end

4.2. Main Controller Design

4.2.1. Main Controller Design of Leader

The virtual error $z_{l,2}$ can be designed as:

$$\begin{cases} z_{l,1} = q_{l,1} - q_{d_{l,1}} \\ z_{l,2} = q_{l,2} - \alpha_{l,1} \end{cases} \tag{13}$$

where $\alpha_{l,1}$ is virtual control.

The uncertainty of the system can be approximated by a fuzzy logic system [58,59] and then an approximation-based controller can be designed as follows.

Theorem 1. *The leader system in Definition 1—(7) can be controlled by the following controller with a predefined accuracy $\mathcal{B}_l = \{z_{l,1} \mid \|z_{l,1}\| \leq \dagger\}$:*

$$\begin{cases} \alpha_{l,1} = -\frac{(2\dagger^2 + \hat{k}_l)z_{l,1}}{2\dagger^2} + \dot{q}_{d_{l,1}} \\ v_l = -g_l(q_{l,1})^{-1} \left(f_l(q_{l,1}, q_{l,2}) + \frac{1}{2} \hat{\theta}_l^T \psi_l(q_{l,1}, q_{l,2}) z_{l,2} + z_{l,1} + \frac{3}{2} z_{l,2} - \dot{\alpha}_{l,1} \right) \\ u_l = U \tanh\left(\frac{v_l}{U}\right) \end{cases} \tag{14}$$

and the adaptive law is

$$\dot{\hat{\theta}}_l = \frac{z_{l,2}^T z_{l,2} \psi_l(q_{l,1}, q_{l,2})}{2} \tag{15}$$

and the adaptive law is

$$\dot{\hat{k}}_l = \frac{z_{l,1}^T z_{l,1}}{2\zeta_l^2 + \dagger^2} \tag{16}$$

where $\hat{\theta}_l = [\hat{\theta}_{l,1}, \dots, \hat{\theta}_{l,n}]^T$ is the adaptive parameter vector. \hat{k}_l is an adaptive parameter and ζ_l is a positive parameter. $\psi_{l,k}(q_{l,1}, q_{l,2}) = \beta_{l,k}(q_{l,1}, q_{l,2})^T \beta_{l,k}(q_{l,1}, q_{l,2})$, and $\psi_l(q_{l,1}, q_{l,2}) = [\psi_{l,1}(q_{l,1}, q_{l,2}), \dots, \psi_{l,n}(q_{l,1}, q_{l,2})]^T$. \dagger is the accuracy parameter.

The proof of Theorem 1 is given in Appendix B.

4.2.2. Main Controller Design of Follower

The virtual error $z_{i,2}$ can be designed as:

$$z_{i,2} = q_{i,2} - \alpha_{i,1} \tag{17}$$

where $\alpha_{i,1}$ is the virtual control.

Theorem 2. *The follower systems in Definition 1—(6) can be controlled by the following controller with a predefined accuracy $\mathcal{B}_i = \{z_{i,1} \mid \|z_{i,1}\| \leq \dagger\}$:*

$$\begin{cases} \alpha_{i,1} = \frac{1}{(b_i + \sum_{h=1}^N a_{ih})} \left(b_i q_{i,2} + \sum_{h=1}^N a_{ih} q_{h,2} - \frac{(2\dagger^2 + \hat{k}_i)z_{i,1}}{2\dagger^2} \right) \\ v_i = -g_i(q_{i,1})^{-1} \left(f_i(q_{i,1}, q_{i,2}) + \frac{1}{2} \hat{\theta}_i^T \psi_i(q_{i,1}, q_{i,2}) z_{i,2} \right. \\ \quad \left. + (b_i + \sum_{h=1}^N a_{ih}) z_{i,1} + \frac{3}{2} z_{i,2} - \dot{\alpha}_{i,1} \right) \\ u_i = U \tanh\left(\frac{v_i}{U}\right) \end{cases} \tag{18}$$

and the adaptive law is

$$\dot{\hat{\theta}}_i = \frac{z_{i,2}^T z_{i,2} \psi_i(q_{i,1}, q_{i,2})}{2} \tag{19}$$

and the adaptive law is

$$\dot{\hat{k}}_i = \frac{z_{i,1}^T z_{i,1}}{2\zeta_i^2 + \dagger^2} \tag{20}$$

where $\hat{\theta}_i = [\hat{\theta}_{i,1}, \dots, \hat{\theta}_{i,n}]^T$ is the adaptive parameter vector. \hat{k}_i is an adaptive parameter and ζ_i is a positive parameter. $\psi_{i,k}(q_{i,1}, q_{i,2}) = \beta_{i,k}(q_{i,1}, q_{i,2})^T \beta_{i,k}(q_{i,1}, q_{i,2})$ and $\psi_i(q_{i,1}, q_{i,2}) = [\psi_{i,1}(q_{i,1}, q_{i,2}), \dots, \psi_{i,n}(q_{i,1}, q_{i,2})]^T$. \dagger is the accuracy parameter.

The proof of Theorem 2 is given in Appendix C.

4.3. Redundant Controller Design

Theorem 3. According to Algorithm 2, the redundant controller can be designed as follows ($i = l, 1, 2, 3, \dots$):

$$\begin{cases} \mathbf{u}_{a_i} = \mathbf{u}_{p_i} & , \text{flag} = 0 \\ \mathbf{u}_{a_i} = \text{Utanh}\left(\frac{v_i}{U}\right) & , \text{flag} = 1 \end{cases} \quad (21)$$

where \mathbf{u}_{p_i} is from (12). When $\text{flag} = 1$, the proof of Theorem 3 is similar to Theorems 1 and 2. The mathematical principle is that the value of u_i and u_{a_i} can be exchanged to obtain a symmetric stability result. According to (A10), (A21) and (21), it is clear that $z_{i,1}$ can converge to a neighborhood of zero $\mathcal{B}_i = \{z_{i,1} \mid \|z_{i,1}\| \leq \dagger\}$ after controller reconstruction.

Algorithm 2 Active fault-tolerant control algorithm ($i = l, 1, 2, 3, \dots$)

Initial stage
 $\mathbf{u}_i = \text{Utanh}\left(\frac{v_i}{U}\right)$
 $\mathbf{u}_{a_i} = \mathbf{u}_{p_i}$
 Switching stage [60]
 If $\text{flag} = 1$
 $\mathbf{u}_i = 0$
 $\mathbf{u}_{a_i} = \text{Utanh}\left(\frac{v_i}{U}\right)$
 end

4.4. Stability Analysis of the System

The Lyapunov functions in (A1) $V_{l,1}$, (A3) $V_{l,2}$, (A11) $V_{i,1}$ and (A14) $V_{i,2}$ are considered to verify the stability of system.

No-fault stage: According to Theorems 1 and 2, it can be deduced that $\dot{V}_{l,1} \leq 0$, $\dot{V}_{l,2} \leq 0$, $\dot{V}_{i,1} \leq 0$ and $\dot{V}_{i,2} \leq 0$ at $\mathbf{q}_{i,1} \in \mathcal{B}_i$. Hence, the system is predefined-accuracy stable.

Fault and no-switching stage: According to Algorithm 1, if $\text{flag} = 0$, $\dot{\mathbf{q}}_{i,2}$ is small and bounded. Then, $\mathbf{q}_{i,2}$ and $\mathbf{q}_{i,1}$ are bounded if the operation time is finite. Next, by considering (8), (13), (14) and (18), and $\mathbf{q}_{d,i,1}$ is bounded, it can be deduced that each virtual error \mathbf{z} is bounded. Then, the Lyapunov functions $V_{l,1} = \mathbf{z}_{l,1}^T \mathbf{z}_{l,1}$, $V_{l,2} = \mathbf{z}_{l,2}^T \mathbf{z}_{l,2}$, $V_{i,1} = \mathbf{z}_{i,1}^T \mathbf{z}_{i,1}$ and $V_{i,2} = \mathbf{z}_{i,2}^T \mathbf{z}_{i,2}$ are also bounded. Hence, according to the above-mentioned bounded inference and Barbalat stability theorem, the system is Lyapunov stable. The steady-state accuracy at this stage can be adjusted by a fault threshold parameter Υ in Algorithm 1.

Switching stage: If the switching is considered as a momentary event [61] and Condition 1 is considered, (A4) can be rewritten as:

$$\begin{aligned} \dot{V}_{l,2} &\leq -\frac{(2^{t^2} + \hat{k}_l) \mathbf{z}_{l,1}^T \mathbf{z}_{l,1}}{2^{t^2}} + \mathbf{z}_{l,1}^T \mathbf{z}_{l,2} + \mathbf{z}_{l,2}^T [f_l(\mathbf{q}_{l,1}, \mathbf{q}_{l,2}) + \Delta f_l(\mathbf{q}_{l,1}, \mathbf{q}_{l,2} - \dot{\mathbf{a}}_{l,1})] \\ &\quad - \tilde{\boldsymbol{\theta}}_l^T \dot{\boldsymbol{\theta}}_l - \tilde{\zeta}_l^2 \tilde{k}_l \hat{k}_l + \left| \mathbf{z}_{l,2}^T \right| |g_l(\mathbf{q}_{l,1}) + \Delta g_l(\mathbf{q}_{l,1})| (|\mathbf{u}_i| + |\mathbf{u}_{a_i}|) \\ &\leq -\frac{(2^{t^2} + \hat{k}_l) \mathbf{z}_{l,1}^T \mathbf{z}_{l,1}}{2^{t^2}} + \mathbf{z}_{l,1}^T \mathbf{z}_{l,2} + \mathbf{z}_{l,2}^T [f_l(\mathbf{q}_{l,1}, \mathbf{q}_{l,2}) + \Delta f_l(\mathbf{q}_{l,1}, \mathbf{q}_{l,2} - \dot{\mathbf{a}}_{l,1})] \\ &\quad - \tilde{\boldsymbol{\theta}}_l^T \dot{\boldsymbol{\theta}}_l - \tilde{\zeta}_l^2 \tilde{k}_l \hat{k}_l + \left| \mathbf{z}_{l,2}^T \right| |g_l(\mathbf{q}_{l,1}) + \Delta g_l(\mathbf{q}_{l,1})| (2U) \end{aligned} \quad (22)$$

Since the virtual errors of the system \mathbf{z} in the fault and no-switching stage are bounded, \dot{V} is bounded. Assuming that the switching time is a very small constant τ . By considering that the Lyapunov functions V in the fault and no-switching stage are also bounded, then $V(t - \tau) + \dot{V}\tau = V(t)$ is bounded. Hence, the leader system is also Lyapunov stable by considering (22).

Redundant control stage: According to Theorem 3, the system is predefined-accuracy stable at $\text{flag} = 1$.

Remark 1. Based on the proposed active fault-detection and redundant fault-tolerance mechanism, the Lyapunov stability analysis of this system can be regarded as continuous. Hence, compared with

other existing fault-tolerant control methods, the proposed method can achieve predefinition of stable accuracy.

5. Simulation

The following simulations are carried out on MATLAB R2016a with a variable simulation step of ode45, 10^{-5} relative tolerance and auto other additional options. A small image embedded in a large image is a local magnification of a large image with the same time scale. Section 5.1 presents the validation simulations of the proposed controller for the single-agent system. Section 5.2 presents the validation simulations of the proposed controller for multi-agent systems with different actuator subsystem faults. Section 5.3 presents comparative simulations between the proposed method and recent passive fault-tolerant methods. Section 5.4 presents the comparative simulations between the proposed method and recent active fault-tolerant methods. This active fault-tolerant method adopts passive fault detection. The structure of multi-agent systems is shown in Figure 3; the subsystem is modeled as the following 2-DOF robot arm system. The advantages of the proposed method can be verified by comparative simulation.

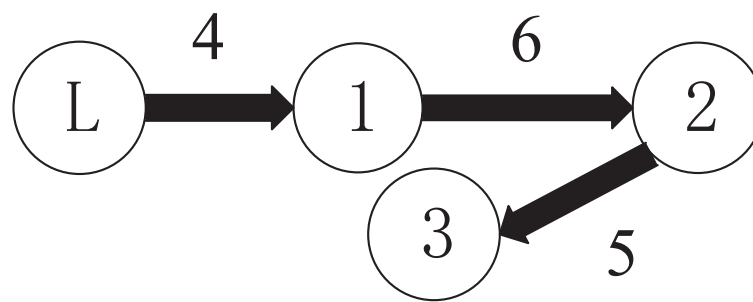


Figure 3. The communication topology of MASs.

According to recent robot studies [62–64], the dynamics of simplified 2-DOF robot arm system are modeled as follows:

$$M(q)\ddot{q} + C(q, \dot{q})\dot{q} + G(q) + D(q) = \tau \quad (23)$$

in which,

$$M(q) = \begin{bmatrix} (m_1 + m_2)l_1^2 + m_2l_2^2 + 2m_2l_1l_2 \cos(q_2) & m_2l_2^2 + m_2l_1l_2 \cos(q_2) \\ m_2l_2^2 + m_2l_1l_2 \cos(q_2) & m_2l_2^2 \end{bmatrix},$$

$$C(q, \dot{q}) = \begin{bmatrix} -2m_2l_1l_2\dot{q}_2 \sin(q_2) & -m_2l_1l_2(\dot{q}_1 + \dot{q}_2) \sin(q_2) \\ m_2l_1l_2\dot{q}_1 \sin(q_2) & 0 \end{bmatrix},$$

$$G(q) = \begin{bmatrix} (m_1 + m_2)gl_1 \cos(q_1) + m_2gl_2 \cos(q_1 + q_2) \\ m_2gl_2 \cos(q_1 + q_2) \end{bmatrix},$$

$$D(q) = \begin{bmatrix} 0.1 \sin(q_1) + 0.1 \cos(q_2) \\ 0.1 \sin(q_2) + 0.1 \cos(q_1) \end{bmatrix},$$

and parameter perturbation is expressed as:

$$\begin{cases} \Delta m_1 = \pm 10\% \\ \Delta m_2 = \pm 10\% \end{cases} \quad (24)$$

where $D(q)$ is disturbance. $g = 9.8 \text{ kg/m}^2$. Mass parameters are $m_1 = 1$ and $m_2 = 0.5$. Link lengths are $l_1 = 1$ and $l_2 = 0.5$.

The initial condition is $[q_1 \quad \dot{q}_1 \quad q_2 \quad \dot{q}_2] = [0.5\pi \quad 0.5\pi \quad 0.5\pi \quad 0.5\pi]$ and the joint angle command is $[q_{d1} \quad q_{d2}] = [\sin(t) + 0.5 \quad \sin(t) + 0.5]$.

The singularity problem of Jacobian matrix $M(q)$ is solved by the DLS method [65]:

$$(M(q))^{-1} = \sum_{i=1}^2 \frac{s_i}{(s_i)^2 + (\zeta_i)^2} \psi_i v_i^T \quad (25)$$

in which

$$\zeta_i = \begin{cases} 0.008(1 + \cos(\frac{\pi s_i}{0.003})), & |s_i| \leq 0.003 \\ 0 & , \text{others} \end{cases}, \quad (26)$$

where $[\nu, s, \psi] = \text{SVD}(M(q))$.

By considering one communication topology structure of MASs as shown in Figure 3, the weighted Laplacian matrix L and weighted adjacency matrix W_1 defined by [66] are shown in the following:

$$\begin{bmatrix} 0 & 0 & 0 \\ 6 \times 1 & 0 & 0 \\ 0 & 5 \times 1 & 0 \end{bmatrix}, \begin{bmatrix} 0 & 0 & 0 \\ 6 \times -1 & 6 \times 1 & 0 \\ 0 & 5 \times -1 & 5 \times 1 \end{bmatrix} \quad (27)$$

with a connected weight matrix of leader and followers

$$\begin{bmatrix} 4 \times 1 & 0 & 0 \\ 0 & 0 & 0 \\ 0 & 0 & 0 \end{bmatrix} \quad (28)$$

The auxiliary input signal is selected as

$$\mathbf{u}_p(t) = \begin{cases} \mathbf{U}_m, & \kappa t_p + t_0 \leq t \leq \kappa t_p + t_0 + \Delta t \\ 0 & , \text{others} \end{cases} \quad (29)$$

where $U_m = 1, t_p = 2, t_0 = 0.5, \Delta t = 0.05$.

The interval type 2 membership function with $\vartheta_r = \bar{\vartheta}_r = \frac{1}{2}$ is chosen as the Gaussian function:

$$\begin{cases} \mu_{\hat{A}_h^L}^L(x_h) = \exp(-\frac{1}{2}(\frac{x_h - m_{h,r}^L}{\sigma_h^r})^2) \\ \mu_{\hat{A}_h^U}^U(x_h) = \exp(-\frac{1}{2}(\frac{x_h - m_{h,r}^U}{\sigma_h^r})^2) \end{cases} \quad (30)$$

where $\sigma_h^r = 1, m_{h,r}^L = -2.1, -1.1, -0.1, 0.9, 1.9, m_{h,r}^U = -1.9, -0.9, 0.1, 1.1, 2.1$.

5.1. Validation Simulations of the Proposed Controller for Single-Agent Systems

In this section, the validation simulation of the proposed method for uncertain single-agent systems is carried out with Condition 1. The model of the single-agent system is based on the leader model of topology-free communication. The initial detector parameter is $Y = 0.1$. The initial parameters are $\dagger = 0.1, U = 30, \hat{\theta}_l(0) = 0, \hat{k}_l(0) = 0.4, \zeta_l = \sqrt{10} \times 10^{-3}$. The actuator fault parameters in Definition 2 are set as follows: $\eta_{l,1} = \eta_{l,2} = 0.05, \omega_{l,1} = \omega_{l,2} = 0.5$ and $t_{a_{l,1}} = t_{a_{l,2}} = 10$.

As shown in Figure 4, it is clear that the tracking error of the proposed method is about 0.05, which is less than the predefined accuracy $\dagger = 0.1$. By considering the simulation results in Figures 4 and 5, there is no significant change in system tracking performance when the fault occurs at 10 s. The reason is the robustness of the control system. Therefore, the auxiliary input in Figure 6 is considered to be added to the control system. According to the results in Figure 5, when the sensor detects the occurrence of acceleration-level abnormal phenomena, Algorithm 1 judges the system failure $flag = 1$ at about 18.55 s. Furthermore, as shown in Figure 7, the maximum absolute values of u_l and u_{a_l} are 30.00 and 27.63, respectively. This result verifies the validity of the constraint controller in Lemma 2.

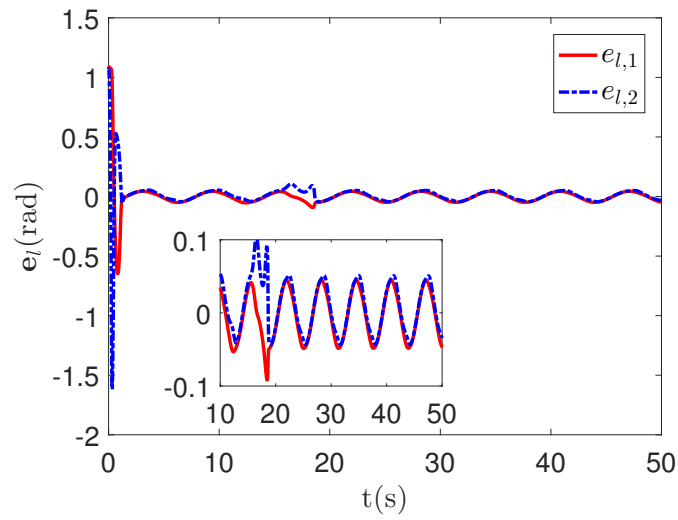


Figure 4. The tracking error curves $e_l = q_{l,1} - q_{d,1}$ of the proposed method.

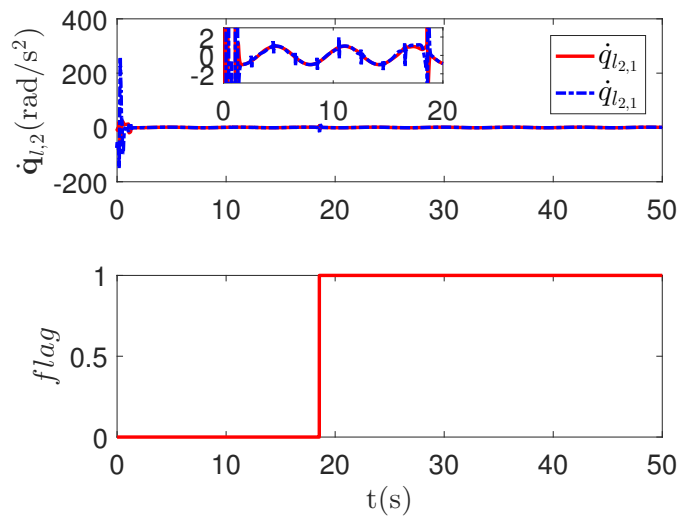


Figure 5. The joint angular acceleration curves $\dot{q}_{l,2}$ and fault-detection curve $Flag$ of the proposed method.

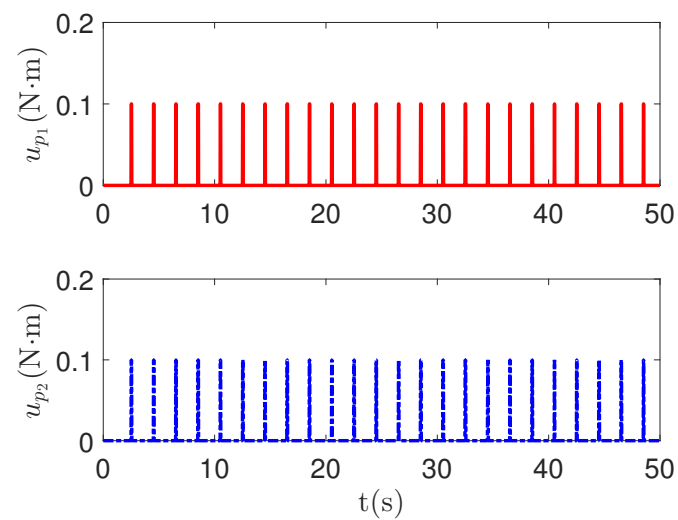


Figure 6. The pulse-wave function curves u_p of the redundant control input u_{a_1} .

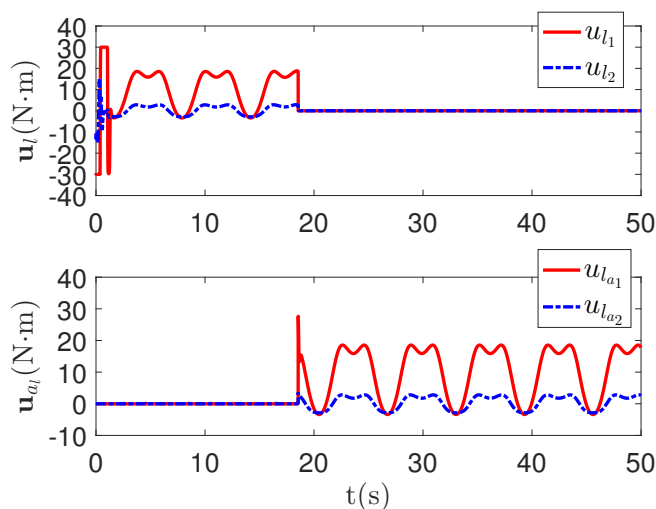


Figure 7. The main control input curves u_l and redundant control input curves u_{a_i} of the proposed method.

5.2. Validation Simulations of the Proposed Controller for Multi-Agent Systems

In this section, the validation simulation of the proposed method for uncertain multi-agent systems is carried out with Condition 1. The initial detector parameter is $Y = 4$. The initial parameters are $\dagger = 0.1$, $U = 30$, $\hat{\theta}_l(0) = \hat{\theta}_i(0) = 0$, $\hat{k}_l(0) = \hat{k}_i(0) = 0.4$, $\zeta_l = \zeta_r = \sqrt{10} \times 10^{-3}$. The actuator fault parameters in Definition 2 are set as follows: $\eta_{1,k} = \omega_{1,k} = t_{a_{1,k}} = \infty$; $\eta_{1,k} = 0.05$, $\omega_{1,k} = 1$, $t_{a_{1,k}} = 20$; $\eta_{2,k} = 0.05$, $\omega_{2,k} = 1.5$, $t_{a_{2,k}} = 30$; $\eta_{3,k} = 0.05$, $\omega_{3,k} = 0.5$, $t_{a_{3,k}} = 10$.

As shown in Figure 8, it is clear that the final tracking error of the proposed method is about 0.02 at 50 s, which is less than the predefined accuracy $\dagger = 0.1$. According to the results in Figures 9 and 10, under three different fault types, the proposed method successfully carries out the corresponding fault detection and controller reconstruction of three followers. When the sensor detects the occurrence of acceleration-level abnormal phenomena, Algorithm 1 judges the system failure $flag = 1$ at about 36.55 s, 36.55 s and 24.55 s, respectively. Meanwhile, the detector is not triggered by mistake for the leader $flag = 0$. Furthermore, as shown in Figures 9 and 10, the maximum absolute values of u_i and u_{a_i} are 30.00 and 30.00, respectively. This result verifies the validity of the constraint controller in Lemma 2.

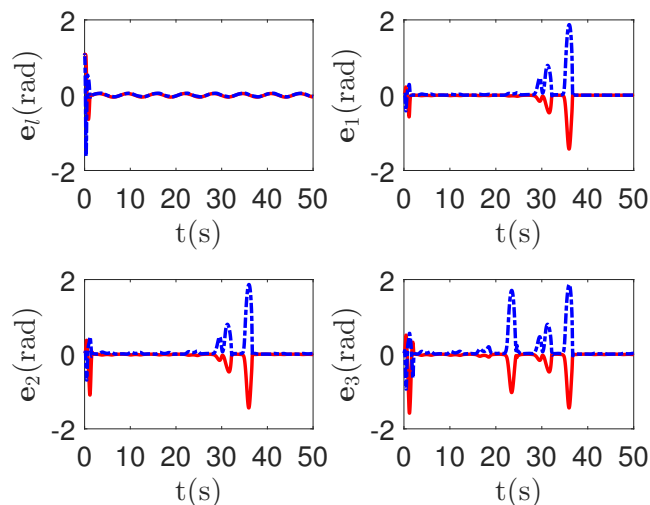


Figure 8. The tracking error curves of leader $e_l = q_{l,1} - q_{d,1}$ and followers $e_i = q_{i,1} - q_{l,1}$ for the proposed method with different actuator faults of subsystems. Figure legends: —: $e_{i,1}, i = l, 1, 2, 3$; - - -: $e_{i,2}, i = l, 1, 2, 3$.

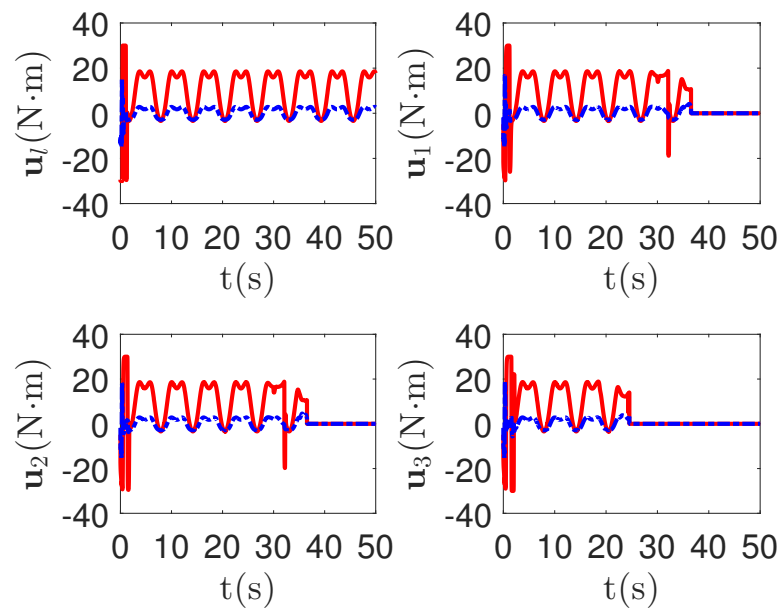


Figure 9. The tracking error curves of leader $u_l = [u_{l,1}, u_{l,2}]^T$ and followers $u_i = [u_{i,1}, u_{i,2}]^T$ for the proposed method with different actuator faults of subsystems. *Figure legends:* —: $u_{i,1}, i = 1, 2, 3$; - - -: $u_{i,2}, i = 1, 2, 3$.

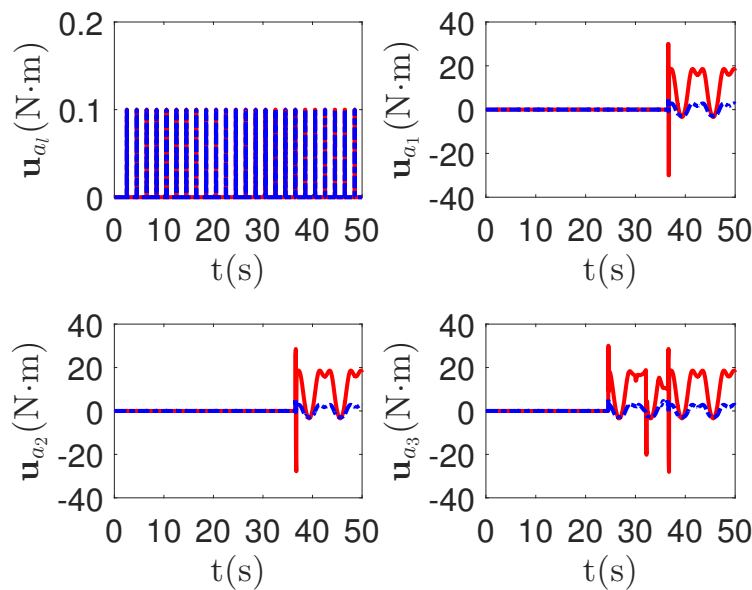


Figure 10. The tracking error curves of leader $u_{a_i} = [u_{a_{i,1}}, u_{a_{i,2}}]^T$ and followers $u_{a_i} = [u_{a_{i,1}}, u_{a_{i,2}}]^T$ for the proposed method with different actuator faults of subsystems. *Figure legends:* —: $u_{a_{i,1}}, i = 1, 2, 3$; - - -: $u_{a_{i,2}}, i = 1, 2, 3$.

5.3. Comparative Simulations between the Proposed Method and the Passive Fault-Tolerant Method

In this section, comparative simulations between the proposed method and the passive fault-tolerant method [67] for uncertain multi-agent systems are carried out with Condition 1. In order to ensure the fairness of the comparison, we use the same fuzzy approximator; the only difference between them is the active detection strategy and passive fault-tolerant strategy. The initial detector parameter is $Y = 4$. The initial parameters are $\dagger = 0.1, U = 30, \hat{\theta}_l(0) = \hat{\theta}_i(0) = 0, \hat{k}_l(0) = \hat{k}_i(0) = 0.4, \zeta_l = \zeta_r = \sqrt{10} \times 10^{-3}$. The actuator fault parameters in Definition 2 are set as follows: $\eta_{l,k} = \eta_{i,k} = 0.05, \omega_{l,k} = \omega_{i,k} = 0.5, t_{a_{l,k}} = t_{a_{i,k}} = 10$.

As shown in Figures 11 and 12, it is clear that the final tracking error of the proposed method is about 0.05 at 50 s, which is less than the predefined accuracy $\dagger = 0.1$. However, the tracking error of passive fault-tolerant control method is not convergent. The reason is that passive fault-tolerant controllers can only operate under minor actuator failures. If the fault function $\Psi_{i,k}(q_{i,1,k}, t)$ is too small, the more master control input is required. However, by considering the control input constraint in Condition 1, the control system can not be stable.

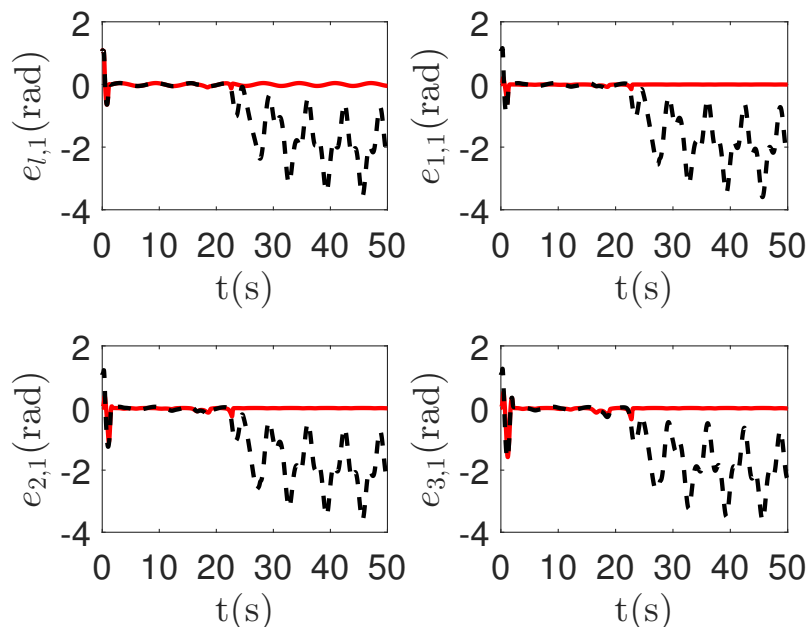


Figure 11. The tracking error curves of leader $e_{l,1} = q_{l,1,1} - q_{d,1,1}$ and followers $e_{i,1} = q_{i,1,1} - q_{l,1,1}$ in the proposed method and passive fault-tolerant control method [67]. Figure legends: —: The proposed method; - - - -: The passive fault-tolerant control method [67].

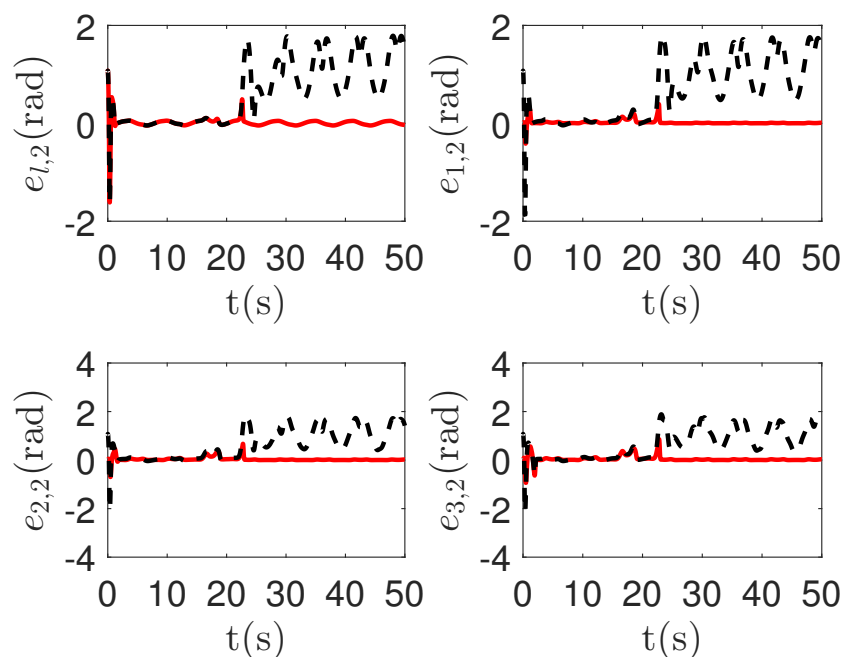


Figure 12. The tracking error curves of leader $e_{l,2} = q_{l,1,2} - q_{d,1,2}$ and followers $e_{i,2} = q_{i,1,2} - q_{l,1,2}$ in the proposed method and passive fault-tolerant control method [67]. Figure legends: —: The proposed method; - - - -: The passive fault-tolerant control method [67].

5.4. The Comparative Simulations between the Proposed Method and Active Fault-Tolerant Method

In this section, the comparative simulations between the proposed method and active fault-tolerant method [68] for uncertain multi-agent systems is carried out with Condition 1. This active fault-tolerant method [68] adopts the passive fault-detection algorithm. In order to ensure the fairness of the comparison, we use the same main controller and adjust similar tracking accuracy. The only difference is that the active and passive detection mechanism. As shown in Figures 13 and 14, the final tracking errors of the two algorithms are similar. The initial detector parameter is $Y = 4$. The initial parameters are $\dagger = 0.1$, $U = 30$, $\hat{\theta}_i(0) = \hat{\theta}_i(0) = 0$, $\hat{k}_l(0) = \hat{k}_i(0) = 0.4$, $\xi_l = \xi_r = \sqrt{10} \times 10^{-3}$. The actuator fault parameters in Definition 2 are set as follows: $\eta_{l,k} = \eta_{i,k} = 0.05$, $\omega_{l,k} = \omega_{i,k} = 0.5$, $t_{a_{l,k}} = t_{a_{i,k}} = 10$.

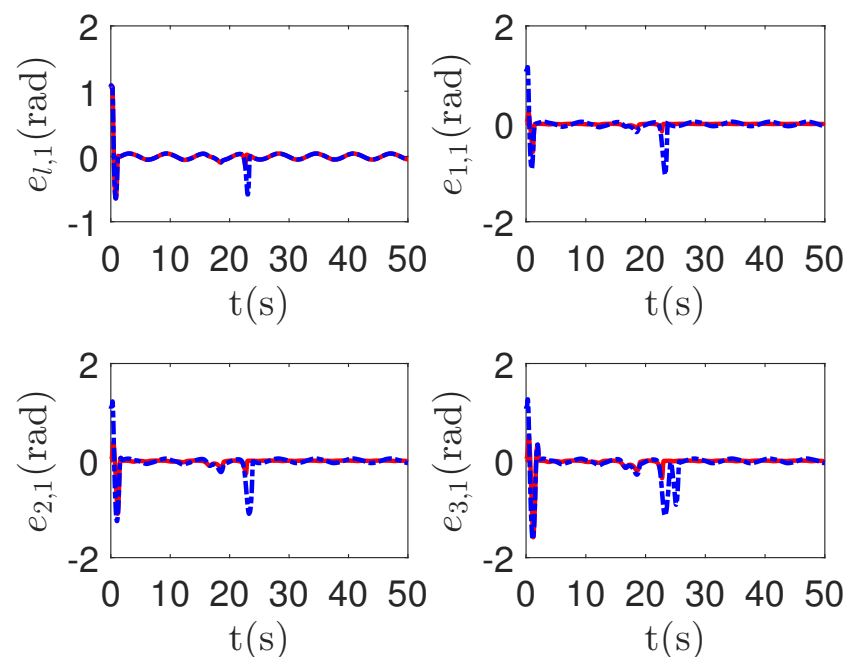


Figure 13. The tracking error curves of leader $e_{l,1} = q_{l,1,1} - q_{d,1,1}$ and followers $e_{i,1} = q_{i,1,1} - q_{l,1,1}$ in the proposed method and passive fault-detection control method [68]. Figure legends: —: The proposed method; - - - -: The active fault-tolerant control method with passive fault detection [68].

As shown in Figures 13 and 14, when the switch happens, the maximum absolute values of tracking errors in the proposed control method are $[0.12, 0.49]^T$, $[0.15, 0.39]^T$, $[0.27, 0.67]^T$ and $[0.36, 0.86]^T$, respectively. When the switch happens, the maximum absolute values of tracking errors in the compared control method [68] are $[0.58, 1.33]^T$, $[1.04, 1.84]^T$, $[1.09, 1.91]^T$ and $[1.13, 1.94]^T$, respectively. It is clear that the system tracking performance of the proposed method is better than that of the passive detection method when switching occurs. According to the results in Figures 15 and 16, the chattering of the proposed main controller is weaker than that of the compared control method during switching. In Figures 17 and 18, the chattering of the proposed main controller is basically weaker than that of the compared control method during switching. Furthermore, according to Figures 15–18, under the same fault, the proposed active fault detector basically detects the fault occurrence at 22.55 s. The compared passive fault detector detects the fault occurrence at 22.91 s, 23.25 s, 23.60 s and 24.90, respectively. This simulation result means that passive detection is more susceptible to topology communication interference of multi-agent systems than active detection.

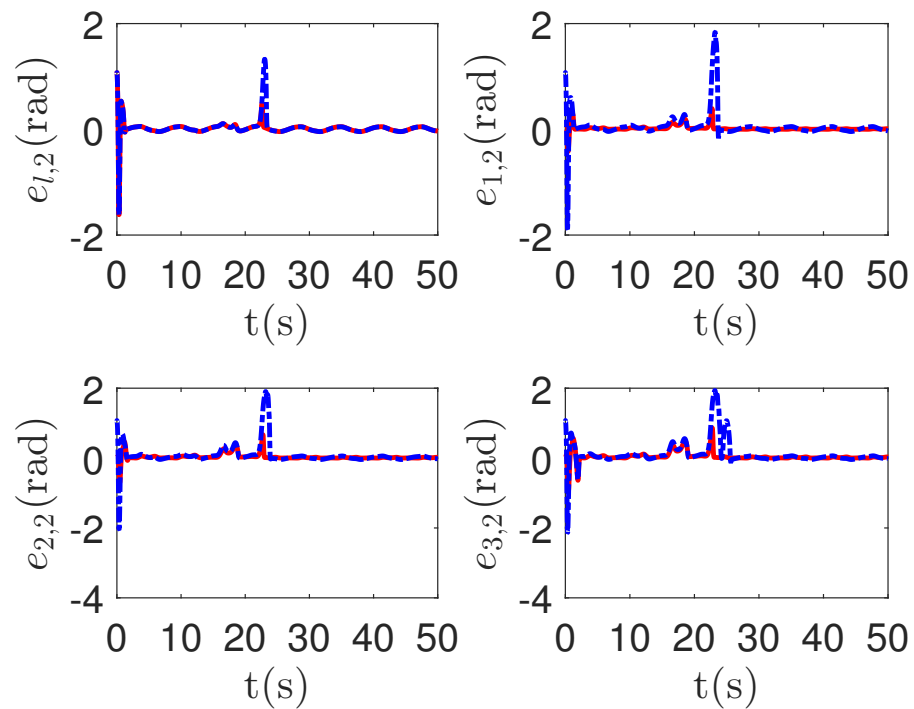


Figure 14. The tracking error curves of leader $e_{l,2} = q_{l,1,2} - q_{d,1,2}$ and followers $e_{i,2} = q_{i,1,2} - q_{l,1,2}$ in the proposed method and passive fault-detection control method [68]. Figure legends: —: The proposed method; - - -: The active fault-tolerant control method with passive fault detection [68].

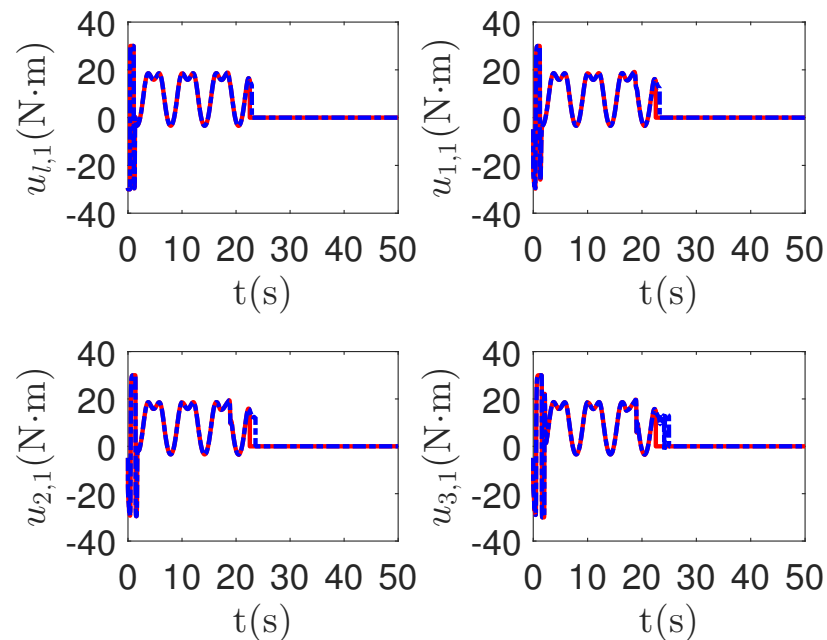


Figure 15. The main control input curves of leader $u_{l,1}$ and followers $u_{i,1}$ in the proposed method and passive fault-detection control method [68]. Figure legends: —: The proposed method; - - -: The active fault-tolerant control method with passive fault detection [68].

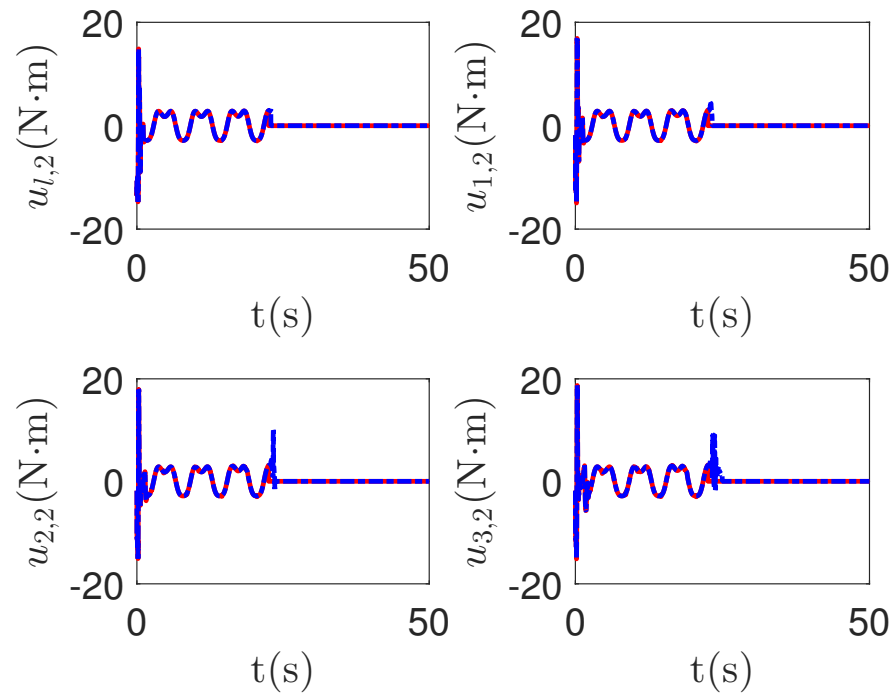


Figure 16. The main control input curves of leader $u_{l,2}$ and followers $u_{i,2}$ in the proposed method and passive fault-detection control method [68]. Figure legends: —: The proposed method; - - -: The active fault-tolerant control method with passive fault detection [68].

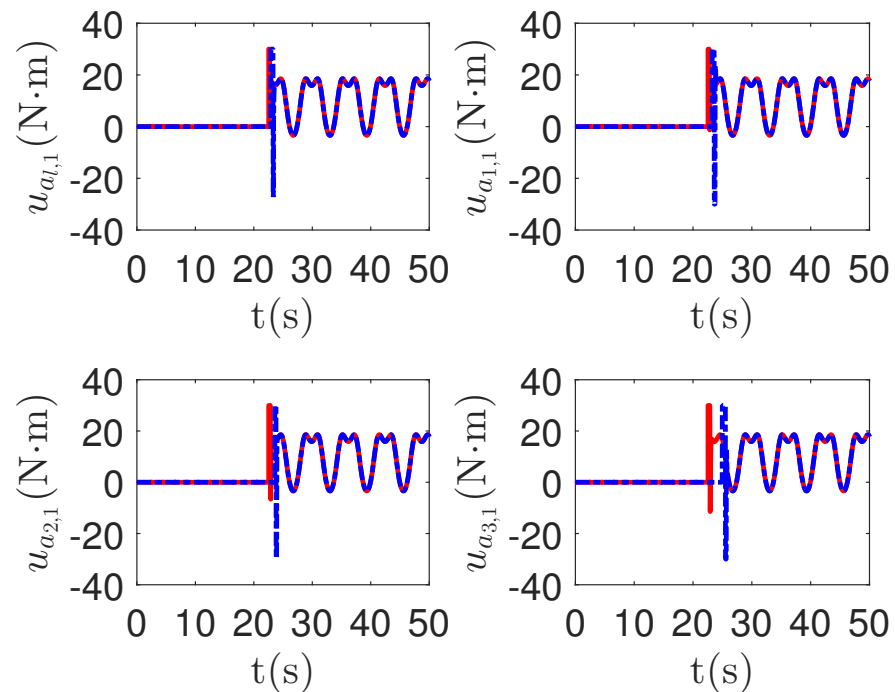


Figure 17. The redundant control input curves of leader $u_{a_{l,1}}$ and followers $u_{a_{i,1}}$ in the proposed method and passive fault-detection control method [68]. Figure legends: —: The proposed method; - - -: The active fault-tolerant control method with passive fault detection [68].

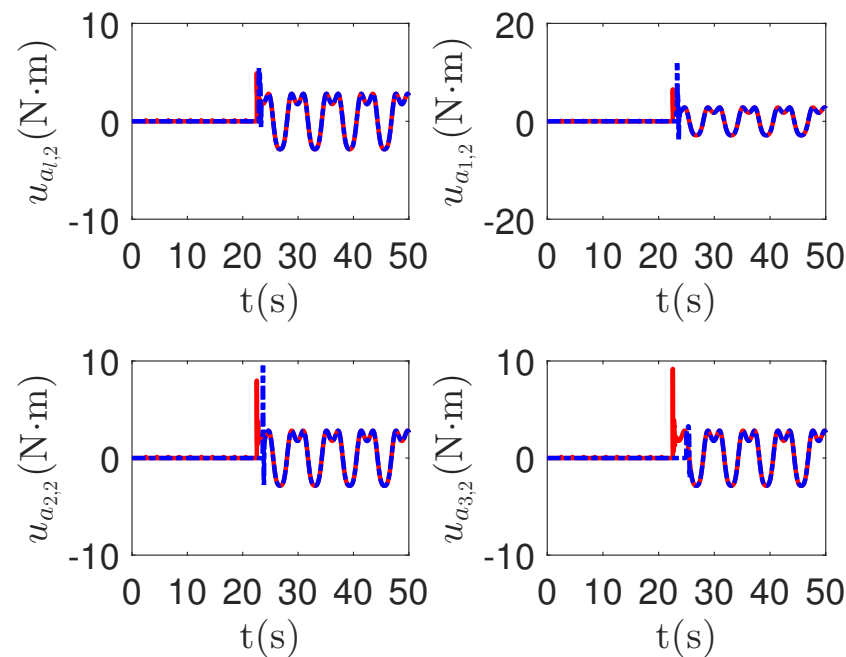


Figure 18. The redundant control input curves of leader $u_{a_{1,2}}$ and followers $u_{a_{i,2}}$ in the proposed method and passive fault-detection control method [68]. *Figure legends:* —: The proposed method; - - -: The active fault-tolerant control method with passive fault detection [68].

6. Conclusions

A novel adaptive interval Type-II fuzzy fault-tolerant control method was proposed for constrained uncertain 2-DOF robotic multi-agent systems by considering an active fault-detection algorithm. This control method can realize the predefined-accuracy stability of multi-agent systems under input saturation, complex actuator failure and high-order system uncertainties. Firstly, a novel active fault-detection algorithm based on pulse-wave function was proposed to detect the failure time of multi-agent systems for the first time. Compared with the existing passive fault-detection methods, the novel active detection algorithm can resist more topology communication interference than passive detection. Then, an improved fault-tolerant control algorithm was adopted to deal with more complex actuator failures. In the end, based on the interval Type-II fuzzy approximated system, a novel adaptive fuzzy fault-tolerant controller was proposed for constrained uncertain mechanical multi-agent systems to achieve predefined-accuracy stability. Compared with other fault-tolerant control methods, the proposed method can achieve predefined-accuracy stability of multi-agent systems under complex multi-agent faults. Meanwhile, the switching chattering of the controller was weaker. These theoretical results were verified by simulation.

Author Contributions: Conceptualization, W.Y. and H.T.; methodology, W.Y.; software, W.Y.; validation, W.Y., H.T. and P.Q.; investigation, W.Y.; resources, H.T.; writing—original draft preparation, W.Y.; writing—review and editing, W.Y., H.T., P.Q. and T.Z.; visualization, W.Y.; supervision, H.T.; funding acquisition, H.T. All authors have read and agreed to the published version of the manuscript.

Funding: This research was funded by the Science and Technology Department of Sichuan Province (No. 2020YFG0119).

Institutional Review Board Statement: Not applicable.

Informed Consent Statement: Not applicable.

Data Availability Statement: Data sharing not applicable.

Conflicts of Interest: The authors declare no conflict of interest.

Appendix A

Graph theory [66]: The topological structure of a multi-agent system is represented by one directed graph $G = (V, E)$, where $V = \{v_1 \dots v_n\}$ and $E \subseteq V \times V$. v_i is a node which represents agent i . If v_i only gets information from v_j , $e_{ji} = (v_j, v_i) \in E$ can be true. v_j represents the neighbor of v_i . $N_i = \{v_j | (v_j, v_i) \in E\}$ represents a collection of v_j . If weights are considered, the proposed graph is a weighted graph. Adjacency matrix $W_1 = [w_{1,ij}] \in R^{N \times N}$ is also the weighted topology. $w_{1,ij} > 0$ if $e_{ji} = (v_j, v_i) \in E$, otherwise $w_{1,ij} = 0$. $D = \text{diag}(d_1, d_2, \dots, d_N) \in R^{N \times N}$, where $d_i = \sum_{j=1}^N w_{1,ij}$ is in-degree of v_i . The Laplacian matrix is $L = D - A$. The communication topology is described by augmented graph $\bar{G} = (\bar{V}, \bar{E})$. There are one leader and N followers.

Appendix B

Proof. Step 1: Consider a candidate Lyapunov function:

$$V_{l,1} = \frac{z_{l,1}^T z_{l,1}}{2} \quad (\text{A1})$$

By considering (13) and (14), the time derivative of Lyapunov function (A1) can be deduced as:

$$\begin{aligned} \dot{V}_{l,1} &= z_{l,1}^T \dot{z}_{l,1} \\ &= z_{l,1}^T \left(q_{l,2} - \dot{q}_{d_{l,1}} \right) \\ &= z_{l,1}^T \left(z_{l,2} + \alpha_{l,1} - \dot{q}_{d_{l,1}} \right) \\ &= -\frac{(2t^2 + \hat{k}_l) z_{l,1}^T z_{l,1}}{2t^2} + z_{l,1}^T z_{l,2} \end{aligned} \quad (\text{A2})$$

Step 2: Consider a candidate Lyapunov function:

$$V_{l,2} = V_{l,1} + \frac{z_{l,2}^T z_{l,2}}{2} + \frac{\tilde{\theta}_l^T \tilde{\theta}_l}{2} + \frac{\tilde{\zeta}_l^2 \tilde{k}_l^2}{2} \quad (\text{A3})$$

where $\tilde{\theta}_l = \theta_l - \hat{\theta}_l$, $\tilde{k}_l = k_l - \hat{k}_l$, in which $k_l \geq \delta_l^T \delta_l + 1$ is defined in (A7).

By considering Lemma 2, (7) and (13), the time derivative of Lyapunov function (A3) can be deduced as:

$$\begin{aligned} \dot{V}_{l,2} &= -\frac{(2t^2 + \hat{k}_l) z_{l,1}^T z_{l,1}}{2t^2} + z_{l,1}^T z_{l,2} + z_{l,2}^T \dot{z}_{l,2} + \tilde{\theta}_l^T (-\dot{\hat{\theta}}_l) + \tilde{\zeta}_l^2 \tilde{k}_l (-\dot{\hat{k}}_l) \\ &= -\frac{(2t^2 + \hat{k}_l) z_{l,1}^T z_{l,1}}{2t^2} + z_{l,1}^T z_{l,2} + z_{l,2}^T [f_l(q_{l,1}, q_{l,2}) + \Delta f_l(q_{l,1}, q_{l,2}) \\ &\quad + (g_l(q_{l,1}) + \Delta g_l(q_{l,1})) (v_l - e(v_l) + u_{a_l}) - \dot{\alpha}_{l,1}] - \tilde{\theta}_l^T \dot{\hat{\theta}}_l - \tilde{\zeta}_l^2 \tilde{k}_l \dot{\hat{k}}_l \end{aligned} \quad (\text{A4})$$

where $e(v_l) = [e_1(v_{l,1}), \dots, e_n(v_{l,n})]^T$.

By considering (14), (A4) can be deduced as:

$$\begin{aligned} \dot{V}_{l,2} &= -\frac{(2t^2 + \hat{k}_l) z_{l,1}^T z_{l,1}}{2t^2} + z_{l,1}^T z_{l,2} + z_{l,2}^T [f_l(q_{l,1}, q_{l,2}) + \Delta f_l(q_{l,1}, q_{l,2}) + \Delta g_l(q_{l,1}) (v_l \\ &\quad - e(v_l) + u_{a_l}) + g_l(q_{l,1}) \left[-g_l(q_{l,1})^{-1} \left(f_l(q_{l,1}, q_{l,2}) + \frac{1}{2} \tilde{\theta}_l^T \psi_l(q_{l,1}, q_{l,2}) z_{l,2} \right. \right. \\ &\quad \left. \left. + z_{l,1} + \frac{3}{2} z_{l,2} - \dot{\alpha}_{l,1} \right) - e(v_l) + u_{a_l} \right] - \dot{\alpha}_{l,1}] - \tilde{\theta}_l^T \dot{\hat{\theta}}_l - \tilde{\zeta}_l^2 \tilde{k}_l \dot{\hat{k}}_l \\ &= -\frac{(2t^2 + \hat{k}_l) z_{l,1}^T z_{l,1}}{2t^2} + z_{l,2}^T [\Delta f_l(q_{l,1}, q_{l,2}) + \Delta g_l(q_{l,1}) (v_l - e(v_l) + u_{a_l}) \\ &\quad + g_l(q_{l,1}) (u_{a_l} - e(v_l))] - \frac{1}{2} z_{l,2}^T \tilde{\theta}_l^T \psi_l(q_{l,1}, q_{l,2}) z_{l,2} - \frac{3}{2} z_{l,2}^T z_{l,2} - \tilde{\theta}_l^T \dot{\hat{\theta}}_l - \tilde{\zeta}_l^2 \tilde{k}_l \dot{\hat{k}}_l \\ &\leq -\frac{(2t^2 + \hat{k}_l) z_{l,1}^T z_{l,1}}{2t^2} - \frac{3}{2} z_{l,2}^T z_{l,2} + |z_{l,2}|^T \chi(q_{l,1}, q_{l,2}) \\ &\quad - \frac{1}{2} z_{l,2}^T z_{l,2} \tilde{\theta}_l^T \psi_l(q_{l,1}, q_{l,2}) - \tilde{\theta}_l^T \dot{\hat{\theta}}_l - \tilde{\zeta}_l^2 \tilde{k}_l \dot{\hat{k}}_l \end{aligned} \quad (\text{A5})$$

in which

$$\chi(\mathbf{q}_{l,1}, \mathbf{q}_{l,2}) = |\Delta f_l(\mathbf{q}_{l,1}, \mathbf{q}_{l,2})| + |\Delta g_l(\mathbf{q}_{l,1})|(\mathbf{U} + \mathbf{E} + \mathbf{U}) + |g_l(\mathbf{q}_{l,1})|(\mathbf{U}_m + \mathbf{E}) \tag{A6}$$

where $|\cdot|$ stands for taking the absolute value of each element in the vector or matrix. $\mathbf{U} = [U, \dots, U]_{1 \times n}^T$ and $\mathbf{E} = [E, \dots, E]_{1 \times n}^T$ are constant vectors. $\mathbf{U}_m = [U_m, \dots, U_m]^T$.

According to Lemma 1, $\chi(\mathbf{q}_{l,1}, \mathbf{q}_{l,2})$ can be approximated by an interval Type-II fuzzy logic system:

$$\chi_k(\mathbf{q}_{l,1}, \mathbf{q}_{l,2}) = \mathbf{w}_{l,k}^T \boldsymbol{\beta}_{l,k}(\mathbf{q}_{l,1}, \mathbf{q}_{l,2}) + \delta_k(\mathbf{q}_{l,1}, \mathbf{q}_{l,2}) \tag{A7}$$

where $\chi(\mathbf{q}_{l,1}, \mathbf{q}_{l,2}) = [\chi_1(\mathbf{q}_{l,1}, \mathbf{q}_{l,2}), \dots, \chi_n(\mathbf{q}_{l,1}, \mathbf{q}_{l,2})]^T$. $|\delta_k(\mathbf{q}_{l,1}, \mathbf{q}_{l,2})| \leq \delta_{l,k}$. $\delta_{l,k}$ is an arbitrary small bounded parameter and the boundary is defined as: $\delta_l^T \delta_l + 1 \leq k_l$. $\delta_l = [\delta_{l,1}, \dots, \delta_{l,n}]^T$.

Then, by considering AM–GM inequality, matrix transformation and (A7), (A5) can be written as:

$$\begin{aligned} \dot{V}_{l,2} \leq & -\frac{(2\ddagger^2 + \hat{k}_l)z_{l,1}^T z_{l,1}}{2\ddagger^2} - \frac{3}{2}z_{l,2}^T z_{l,2} + \frac{1}{2} + \frac{z_{l,2}^T z_{l,2} \boldsymbol{\theta}_l^T \boldsymbol{\psi}_l(\mathbf{q}_{l,1}, \mathbf{q}_{l,2})}{2} + \frac{z_{l,2}^T z_{l,2}}{2} + \frac{\delta_l^T \delta_l}{2} \\ & - \frac{1}{2}z_{l,2}^T z_{l,2} (\boldsymbol{\theta}_l^T - \tilde{\boldsymbol{\theta}}_l^T) \boldsymbol{\psi}_l(\mathbf{q}_{l,1}, \mathbf{q}_{l,2}) - \tilde{\boldsymbol{\theta}}_l^T \hat{\boldsymbol{\theta}}_l - \tilde{\zeta}_l^2 \tilde{k}_l \hat{k}_l \end{aligned} \tag{A8}$$

where $\theta_{l,k} = \mathbf{w}_{l,k}^T \boldsymbol{\beta}_{l,k}$ and $\boldsymbol{\theta}_l = [\theta_{l,1}, \dots, \theta_{l,n}]^T$.

Then, by substituting (15), (A8) can be written as:

$$\begin{aligned} \dot{V}_{l,2} \leq & -\frac{(2\ddagger^2 + \hat{k}_l)z_{l,1}^T z_{l,1}}{2\ddagger^2} - z_{l,2}^T z_{l,2} + \frac{1}{2} + \frac{\delta_l^T \delta_l}{2} \\ & + \frac{z_{l,2}^T z_{l,2} \tilde{\boldsymbol{\theta}}_l^T \boldsymbol{\psi}_l(\mathbf{q}_{l,1}, \mathbf{q}_{l,2})}{2} - \tilde{\boldsymbol{\theta}}_l^T \left(\frac{z_{l,2}^T z_{l,2} \boldsymbol{\psi}_l(\mathbf{q}_{l,1}, \mathbf{q}_{l,2})}{2} \right) - \tilde{\zeta}_l^2 \tilde{k}_l \hat{k}_l \\ \leq & -z_{l,1}^T z_{l,1} - z_{l,2}^T z_{l,2} - \frac{(k_l - \tilde{k}_l)z_{l,1}^T z_{l,1}}{2\ddagger^2} + \frac{1 + \delta_l^T \delta_l}{2} - \tilde{\zeta}_l^2 \tilde{k}_l \hat{k}_l \end{aligned} \tag{A9}$$

Then, by substituting (16), (A9) can be written as:

$$\begin{aligned} \dot{V}_{l,2} \leq & -z_{l,1}^T z_{l,1} - z_{l,2}^T z_{l,2} + \frac{k_l}{2} \left(1 - \frac{z_{l,1}^T z_{l,1}}{\ddagger^2} \right) + \frac{\tilde{k}_l z_{l,1}^T z_{l,1}}{2\ddagger^2} - \tilde{\zeta}_l^2 \tilde{k}_l \frac{z_{l,1}^T z_{l,1}}{2\tilde{\zeta}_l^2 \ddagger^2} \\ \leq & -z_{l,1}^T z_{l,1} - z_{l,2}^T z_{l,2} + \frac{k_l}{2} \left(1 - \frac{z_{l,1}^T z_{l,1}}{\ddagger^2} \right) \end{aligned} \tag{A10}$$

According to (A10), it is clear that $z_{l,1}$ can converge to a neighborhood of zero $\mathcal{B}_l = \{z_{l,1} \mid \|z_{l,1}\| \leq \ddagger\}$ if there is no actuator fault.

The proof is completed. \square

Appendix C

Proof. Step 1: Consider a candidate Lyapunov function:

$$V_{i,1} = \frac{z_{i,1}^T z_{i,1}}{2} \tag{A11}$$

By considering (8), the time derivative of Lyapunov function (A11) can be deduced as:

$$\begin{aligned} \dot{V}_{i,1} &= z_{i,1}^T \dot{z}_{i,1} \\ &= z_{i,1}^T \left[\left(b_i + \sum_{h=1}^N a_{ih} \right) (z_{i,2} + \boldsymbol{\alpha}_{i,1}) - b_i \mathbf{q}_{l,2} - \sum_{h=1}^N a_{ih} \mathbf{q}_{h,2} \right] \end{aligned} \tag{A12}$$

By considering (18), (A12) can be deduced as:

$$\begin{aligned} \dot{V}_{i,1} &= z_{i,1}^T \left[\left(b_i + \sum_{h=1}^N a_{ih} \right) \left(z_{i,2} + \frac{1}{(b_i + \sum_{h=1}^N a_{ih})} \left(b_i \mathbf{q}_{l,2} + \sum_{h=1}^N a_{ih} \mathbf{q}_{h,2} - \frac{(2\ddagger^2 + \hat{k}_i)z_{i,1}}{2\ddagger^2} \right) \right) \right. \\ &\quad \left. - b_i \mathbf{q}_{l,2} - \sum_{h=1}^N a_{ih} \mathbf{q}_{h,2} \right] \\ &= -\frac{(2\ddagger^2 + \hat{k}_i)z_{i,1}^T z_{i,1}}{2\ddagger^2} + \left(b_i + \sum_{h=1}^N a_{ih} \right) z_{i,1}^T z_{i,2} \end{aligned} \tag{A13}$$

Step 2: Consider a candidate Lyapunov function:

$$V_{i,2} = V_{i,1} + \frac{z_{i,2}^T z_{i,2}}{2} + \frac{\tilde{\theta}_i^T \tilde{\theta}_i}{2} + \frac{\tilde{\zeta}_i^2 \tilde{k}_i^2}{2} \quad (\text{A14})$$

where $\tilde{\theta}_i = \theta_i - \hat{\theta}_i$, $\tilde{k}_i = k_i - \hat{k}_i$, in which $k_i \geq \delta_i^T \delta_i + 1$ is defined in (A18).

By considering Lemma 2, (6) and (17), the time derivative of Lyapunov function (A14) can be deduced as:

$$\begin{aligned} \dot{V}_{i,2} &= -\frac{(2^{+2} + \hat{k}_i) z_{i,1}^T z_{i,1}}{2^{+2}} + \left(b_i + \sum_{h=1}^N a_{ih} \right) z_{i,1}^T z_{i,2} + z_{i,2}^T \dot{z}_{i,2} + \tilde{\theta}_i^T (-\dot{\hat{\theta}}_i) + \tilde{\zeta}_i^2 \tilde{k}_i (-\dot{\hat{k}}_i) \\ &= -\frac{(2^{+2} + \hat{k}_i) z_{i,1}^T z_{i,1}}{2^{+2}} + \left(b_i + \sum_{h=1}^N a_{ih} \right) z_{i,1}^T z_{i,2} + z_{i,2}^T [f_i(q_{i,1}, q_{i,2}) + \Delta f_i(q_{i,1}, q_{i,2}) \\ &\quad + (g_i(q_{i,1}) + \Delta g_i(q_{i,1}))(v_i - e(v_i) + u_{a_i}) - \dot{\alpha}_{i,1}] - \tilde{\theta}_i^T \dot{\hat{\theta}}_i - \tilde{\zeta}_i^2 \tilde{k}_i \dot{\hat{k}}_i \end{aligned} \quad (\text{A15})$$

where $e(v_i) = [e_1(v_{i,1}), \dots, e_n(v_{i,n})]^T$.

By considering (18), (A15) can be deduced as:

$$\begin{aligned} \dot{V}_{i,2} &= -\frac{(2^{+2} + \hat{k}_i) z_{i,1}^T z_{i,1}}{2^{+2}} + \left(b_i + \sum_{h=1}^N a_{ih} \right) z_{i,1}^T z_{i,2} + z_{i,2}^T [f_i(q_{i,1}, q_{i,2}) \\ &\quad + \Delta f_i(q_{i,1}, q_{i,2}) + \Delta g_i(q_{i,1})(v_i - e(v_i) + u_{a_i}) \\ &\quad + g_i(q_{i,1}) \left[-g_i(q_{i,1})^{-1} \left(f_i(q_{i,1}, q_{i,2}) + \frac{1}{2} \tilde{\theta}_i^T \psi_i(q_{i,1}, q_{i,2}) z_{i,2} \right. \right. \\ &\quad \left. \left. + \left(b_i + \sum_{h=1}^N a_{ih} \right) z_{i,1} + \frac{3}{2} z_{i,2} - \dot{\alpha}_{i,1} \right) - e(v_i) + u_{a_i} \right] - \dot{\alpha}_{i,1}] - \tilde{\theta}_i^T \dot{\hat{\theta}}_i - \tilde{\zeta}_i^2 \tilde{k}_i \dot{\hat{k}}_i \\ &\leq -\frac{(2^{+2} + \hat{k}_i) z_{i,1}^T z_{i,1}}{2^{+2}} - \frac{3}{2} z_{i,2}^T z_{i,2} + |z_{i,2}|^T \chi(q_{i,1}, q_{i,2}) \\ &\quad - \frac{1}{2} z_{i,2}^T z_{i,2} \tilde{\theta}_i^T \psi_i(q_{i,1}, q_{i,2}) - \tilde{\theta}_i^T \dot{\hat{\theta}}_i - \tilde{\zeta}_i^2 \tilde{k}_i \dot{\hat{k}}_i \end{aligned} \quad (\text{A16})$$

in which

$$\chi(q_{i,1}, q_{i,2}) = |\Delta f_i(q_{i,1}, q_{i,2})| + |\Delta g_i(q_{i,1})|(\mathbf{U} + \mathbf{E} + \mathbf{U}) + |g_i(q_{i,1})|(\mathbf{U}_m + \mathbf{E}) \quad (\text{A17})$$

where $|\cdot|$ stands for taking the absolute value of each element in the vector or matrix. $\mathbf{U} = [U, \dots, U]_{1 \times n}^T$ and $\mathbf{E} = [E, \dots, E]_{1 \times n}^T$ are the constant vectors. $\mathbf{U}_m = [U_m, \dots, U_m]^T$.

According to Lemma 1, $\chi(q_{i,1}, q_{i,2})$ can be approximated by an interval Type-2 fuzzy logic system:

$$\chi_k(q_{i,1}, q_{i,2}) = w_{i,k}^T \beta_{i,k}(q_{i,1}, q_{i,2}) + \delta_k(q_{i,1}, q_{i,2}) \quad (\text{A18})$$

where $\chi(q_{i,1}, q_{i,2}) = [\chi_1(q_{i,1}, q_{i,2}), \dots, \chi_n(q_{i,1}, q_{i,2})]^T$. $|\delta_k(q_{i,1}, q_{i,2})| \leq \delta_{i,k}$. $\delta_{i,k}$ is an arbitrary small bounded parameter and the boundary is defined as: $\delta_i^T \delta_i + 1 \leq k_i$. $\delta_i = [\delta_{i,1}, \dots, \delta_{i,n}]^T$.

Then, by considering AM–GM inequality, matrix transformation and (A18), (A16) can be written as:

$$\begin{aligned} \dot{V}_{i,2} &\leq -\frac{(2^{+2} + \hat{k}_i) z_{i,1}^T z_{i,1}}{2^{+2}} - \frac{3}{2} z_{i,2}^T z_{i,2} + \frac{1^2}{2} + \frac{z_{i,2}^T z_{i,2} \tilde{\theta}_i^T \psi_i(q_{i,1}, q_{i,2})}{2} + \frac{z_{i,2}^T z_{i,2}}{2} + \frac{\delta_i^T \delta_i}{2} \\ &\quad - \frac{1}{2} z_{i,2}^T z_{i,2} (\tilde{\theta}_i^T - \tilde{\theta}_i^T) \psi_i(q_{i,1}, q_{i,2}) - \tilde{\theta}_i^T \dot{\hat{\theta}}_i - \tilde{\zeta}_i^2 \tilde{k}_i \dot{\hat{k}}_i \end{aligned} \quad (\text{A19})$$

where $\theta_{i,k} = w_{i,k}^T w_{i,k}$ and $\theta_i = [\theta_{i,1}, \dots, \theta_{i,n}]^T$.

Then, by substituting (19), (A19) can be written as:

$$\dot{V}_{i,2} \leq -z_{i,1}^T z_{i,1} - z_{i,2}^T z_{i,2} - \frac{(k_i - \tilde{k}_i) z_{i,1}^T z_{i,1}}{2^{+2}} + \frac{1 + \delta_i^T \delta_i}{2} - \tilde{\zeta}_i^2 \tilde{k}_i \dot{\hat{k}}_i \quad (\text{A20})$$

Then, by substituting (20), (A20) can be written as:

$$\dot{V}_{i,2} \leq -z_{i,1}^T z_{i,1} - z_{i,2}^T z_{i,2} + \frac{k_i}{2} \left(1 - \frac{z_{i,1}^T z_{i,1}}{\ddagger} \right) \quad (\text{A21})$$

According to (A21), it is clear that $z_{i,1}$ can converge to a neighborhood of zero $\mathcal{B}_i = \{z_{i,1} \mid \|z_{i,1}\| \leq \ddagger\}$ if there is no actuator fault.

The proof is completed. \square

References

1. Wang, X.; Park, J.H.; Yang, H. An improved protocol to consensus of delayed MASs with UNMS and aperiodic DoS cyber-attacks. *IEEE Trans. Netw. Sci. Eng.* **2021**, *8*, 2506–2516. [[CrossRef](#)]
2. Jiang, Y.; Niu, B.; Wang, X.; Zhao, X.; Wang, H.; Yan, B. Distributed finite-time consensus tracking control for nonlinear multi-agent systems with FDI attacks and application to single-link robots. *IEEE Trans. Circuits Syst. II Express Briefs* **2022**, *70*, 1505–1509. [[CrossRef](#)]
3. Zhang, K.; Zhao, T.; Dian, S. Dynamic output feedback control for nonlinear networked control systems with a two-terminal event-triggered mechanism. *Nonlinear Dyn.* **2020**, *100*, 2537–2555. [[CrossRef](#)]
4. Zhao, T.; Li, H.; Dian, S. Multi-robot path planning based on improved artificial potential field and fuzzy inference system. *J. Intell. Fuzzy Syst.* **2020**, *39*, 7621–7637. [[CrossRef](#)]
5. Chen, W.D.; Li, Y.X.; Liu, L.; Zhao, X.D.; Niu, B.; Han, L.M. Nussbaum-Based Adaptive Fault-Tolerant Control for Nonlinear CPSs With Deception Attacks: A New Coordinate Transformation Technology. *IEEE Trans. Cybern.* **2022**. [[CrossRef](#)] [[PubMed](#)]
6. Wang, H.; Ma, J.; Zhao, X.; Niu, B.; Chen, M.; Wang, W. Adaptive Fuzzy Fixed-Time Control for High-Order Nonlinear Systems With Sensor and Actuator Faults. *IEEE Trans. Fuzzy Syst.* **2023**. [[CrossRef](#)]
7. Amin, A.A.; Hasan, K.M. A review of fault tolerant control systems: Advancements and applications. *Measurement* **2019**, *143*, 58–68. [[CrossRef](#)]
8. Wang, X.; Niu, B.; Song, X.; Zhao, P.; Wang, Z. Neural networks-based adaptive practical preassigned finite-time fault tolerant control for nonlinear time-varying delay systems with full state constraints. *Int. J. Robust Nonlinear Control* **2021**, *31*, 1497–1513. [[CrossRef](#)]
9. Li, Q.; Wu, Q.; Tu, H.; Zhang, J.; Zou, X.; Huang, S. Ground Risk Assessment for Unmanned Aircraft Focusing on Multiple Risk Sources in Urban Environments. *Processes* **2023**, *11*, 542. [[CrossRef](#)]
10. Zhang, Y.; Jiang, J. Bibliographical review on reconfigurable fault-tolerant control systems. *Annu. Rev. Control* **2008**, *32*, 229–252. [[CrossRef](#)]
11. Zhang, Y.; Jiang, J. Active fault-tolerant control system against partial actuator failures. *IEE Proc. Control Theory Appl.* **2002**, *149*, 95–104. [[CrossRef](#)]
12. Maki, M.; Jiang, J.; Hagino, K. A stability guaranteed active fault-tolerant control system against actuator failures. *Int. J. Robust Nonlinear Control IFAC Affil. J.* **2004**, *14*, 1061–1077. [[CrossRef](#)]
13. Merheb, A.R.; Noura, H.; Bateman, F. Active fault tolerant control of quadrotor uav using sliding mode control. In Proceedings of the 2014 International Conference on Unmanned Aircraft Systems (ICUAS), Orlando, FL, USA, 27–30 May 2014; pp. 156–166.
14. Hosseinnajad, A.; Loueipour, M. Design of finite-time active fault tolerant control system with real-time fault estimation for a remotely operated vehicle. *Ocean Eng.* **2021**, *241*, 110063. [[CrossRef](#)]
15. Li, J.; Xiang, X.; Dong, D.; Yang, S. Prescribed time observer based trajectory tracking control of autonomous underwater vehicle with tracking error constraints. *Ocean Eng.* **2023**, *274*, 114018. [[CrossRef](#)]
16. Zhang, J.; Niu, B.; Wang, D.; Wang, H.; Zhao, P.; Zong, G. Time-/event-triggered adaptive neural asymptotic tracking control for nonlinear systems with full-state constraints and application to a single-link robot. *IEEE Trans. Neural Netw. Learn. Syst.* **2021**, *33*, 6690–6700. [[CrossRef](#)]
17. Tang, H.; Gao, S.; Wang, L.; Li, X.; Li, B.; Pang, S. A novel intelligent fault diagnosis method for rolling bearings based on Wasserstein generative adversarial network and Convolutional Neural Network under Unbalanced Dataset. *Sensors* **2021**, *21*, 6754. [[CrossRef](#)]
18. Xiao, L.; Bajric, R.; Zhao, J.; Tang, J.; Zhang, X. An adaptive vibrational resonance method based on cascaded varying stable-state nonlinear systems and its application in rotating machine fault detection. *Nonlinear Dyn.* **2021**, *103*, 715–739. [[CrossRef](#)]
19. Bzioui, S.; Channa, R. Estimation and fault diagnosis for non-linear system with time-varying faults and measurement noises: Application on two CSTRs in series. *Can. J. Chem. Eng.* **2023**, *101*, 1919–1930. [[CrossRef](#)]
20. Gao, Y.; Xiao, F.; Liu, J.; Wang, R. Distributed soft fault detection for interval type-2 fuzzy-model-based stochastic systems with wireless sensor networks. *IEEE Trans. Ind. Inform.* **2018**, *15*, 334–347. [[CrossRef](#)]
21. Hebda-Sobkiewicz, J.; Zimroz, R.; Pitera, M.; Wylomańska, A. Informative frequency band selection in the presence of non-Gaussian noise—A novel approach based on the conditional variance statistic with application to bearing fault diagnosis. *Mech. Syst. Signal Process.* **2020**, *145*, 106971. [[CrossRef](#)]
22. Zhang, G.; Shu, Y.; Zhang, T. Piecewise unsaturated multi-stable stochastic resonance under trichotomous noise and its application in bearing fault diagnosis. *Results Phys.* **2021**, *30*, 104907. [[CrossRef](#)]
23. Stojanovic, V.; Prsic, D. Robust identification for fault detection in the presence of non-Gaussian noises: Application to hydraulic servo drives. *Nonlinear Dyn.* **2020**, *100*, 2299–2313. [[CrossRef](#)]
24. Zhang, G.; Zhang, Y.; Zhang, T.; Mdsheh, R. Stochastic resonance in an asymmetric bistable system driven by multiplicative and additive Gaussian noise and its application in bearing fault detection. *Chin. J. Phys.* **2018**, *56*, 1173–1186. [[CrossRef](#)]
25. Zhao, H.; Yang, X.; Chen, B.; Chen, H.; Deng, W. Bearing fault diagnosis using transfer learning and optimized deep belief network. *Meas. Sci. Technol.* **2022**, *33*, 065009. [[CrossRef](#)]

26. Zhao, H.; Zhang, P.; Zhang, R.; Yao, R.; Deng, W. A novel performance trend prediction approach using ENBLs with GWO. *Meas. Sci. Technol.* **2022**, *34*, 025018. [[CrossRef](#)]
27. Andjelkovic, I.; Sweetingham, K.; Campbell, S.L. Active fault detection in nonlinear systems using auxiliary signals. In Proceedings of the 2008 American Control Conference, Seattle, WA, USA, 11–13 June 2008; pp. 2142–2147.
28. Ashari, A.E.; Nikoukhah, R.; Campbell, S.L. Effects of feedback on active fault detection. *Automatica* **2012**, *48*, 866–872. [[CrossRef](#)]
29. Punčochář, I.; Široký, J.; Šimandl, M. Constrained active fault detection and control. *IEEE Trans. Autom. Control* **2014**, *60*, 253–258. [[CrossRef](#)]
30. Jia, F.; Cao, F.; Lyu, G.; He, X. A novel framework of cooperative design: Bringing active fault diagnosis into fault-tolerant control. *IEEE Trans. Cybern.* **2022**, *53*, 3301–3310. [[CrossRef](#)]
31. Jiang, Y.; Niu, B.; Wang, X.; Wang, H.; Chen, W. Dynamic-estimator-based adaptive secure containment control for constrained nonlinear multi-agent systems under denial-of-service attacks. *Int. J. Robust Nonlinear Control* **2023**, *33*, 605–622. [[CrossRef](#)]
32. Zhao, T.; Dian, S. State feedback control for interval type-2 fuzzy systems with time-varying delay and unreliable communication links. *IEEE Trans. Fuzzy Syst.* **2017**, *26*, 951–966. [[CrossRef](#)]
33. Wang, X.; Park, J.H.; She, K.; Zhong, S.; Shi, L. Stabilization of chaotic systems with T-S fuzzy model and nonuniform sampling: A switched fuzzy control approach. *IEEE Trans. Fuzzy Syst.* **2018**, *27*, 1263–1271. [[CrossRef](#)]
34. Qin, P.; Zhao, T.; Dian, S. Interval type-2 fuzzy neural network-based adaptive compensation control for omni-directional mobile robot. *Neural Comput. Appl.* **2023**, 1–15. [[CrossRef](#)]
35. Zhao, J.; Zhao, T.; Liu, N. Fractional-Order Active Disturbance Rejection Control with Fuzzy Self-Tuning for Precision Stabilized Platform. *Entropy* **2022**, *24*, 1681. [[CrossRef](#)] [[PubMed](#)]
36. Xiu, Z.; Wang, Y.; Cheng, Z. Stability analysis and design of Type-II fuzzy controllers. In Proceedings of the 2008 Chinese Control and Decision Conference, Yantai, China, 2–4 July 2008; pp. 2054–2059.
37. Mohagheghi, S.; Venayagamoorthy, G.K.; Harley, R.G. An interval Type-II robust fuzzy logic controller for a static compensator in a multimachine power system. In Proceedings of the 2006 IEEE International Joint Conference on Neural Network Proceedings, Vancouver, BC, Canada, 16–21 July 2006; pp. 2241–2248.
38. Tang, F.; Niu, B.; Wang, H.; Zhang, L.; Zhao, X. Adaptive fuzzy tracking control of switched MIMO nonlinear systems with full state constraints and unknown control directions. *IEEE Trans. Circuits Syst. Express Briefs* **2022**, *69*, 2912–2916. [[CrossRef](#)]
39. Dian, S.; Hu, Y.; Zhao, T.; Han, J. Adaptive backstepping control for flexible-joint manipulator using interval type-2 fuzzy neural network approximator. *Nonlinear Dyn.* **2019**, *97*, 1567–1580. [[CrossRef](#)]
40. Tong, W.; Zhao, T.; Duan, Q.; Zhang, H.; Mao, Y. Non-singleton interval type-2 fuzzy PID control for high precision electro-optical tracking system. *ISA Trans.* **2022**, *120*, 258–270. [[CrossRef](#)]
41. Wang, J.; Hu, L.; Chen, F.; Wen, C. Multiple-step fault estimation for interval type-II TS fuzzy system of hypersonic vehicle with time-varying elevator faults. *Int. J. Adv. Robot. Syst.* **2017**, *14*, 1729881417699149. [[CrossRef](#)]
42. Patel, H.; Shah, V. Actuator and system component fault tolerant control using interval type-2 Takagi-Sugeno fuzzy controller for hybrid nonlinear process. *Int. J. Hybrid Intell. Syst.* **2019**, *15*, 143–153. [[CrossRef](#)]
43. Yeh, C.C.; Demerdash, N.A. Fault-tolerant soft starter control of induction motors with reduced transient torque pulsations. *IEEE Trans. Energy Convers.* **2009**, *24*, 848–859.
44. Yang, L.; Ozay, N. Fault-tolerant output-feedback path planning with temporal logic constraints. In Proceedings of the 2018 IEEE Conference on Decision and Control (CDC), Miami, FL, USA, 17–19 December 2018; pp. 4032–4039.
45. Li, Z.; Jamshidian, M.; Mousavi, S.; Karimpour, A.; Tlili, I. Develop a numerical approach of fuzzy logic type-2 to improve the reliability of a hydraulic automated guided vehicles. *Int. J. Numer. Methods Heat Fluid Flow* **2021**, *31*, 1396–1409. [[CrossRef](#)]
46. Lin, M.; Huang, C.; Xu, Z.; Chen, R. Evaluating IoT platforms using integrated probabilistic linguistic MCDM method. *IEEE Internet Things J.* **2020**, *7*, 11195–11208. [[CrossRef](#)]
47. Huang, C.; Lin, M.; Xu, Z. Pythagorean fuzzy MULTIMOORA method based on distance measure and score function: Its application in multicriteria decision making process. *Knowl. Inf. Syst.* **2020**, *62*, 4373–4406. [[CrossRef](#)]
48. Lin, M.; Huang, C.; Xu, Z. TOPSIS method based on correlation coefficient and entropy measure for linguistic Pythagorean fuzzy sets and its application to multiple attribute decision making. *Complexity* **2019**, *2019*, 6967390. [[CrossRef](#)]
49. Lin, M.; Wang, H.; Xu, Z. TODIM-based multi-criteria decision-making method with hesitant fuzzy linguistic term sets. *Artif. Intell. Rev.* **2020**, *53*, 3647–3671. [[CrossRef](#)]
50. Lin, M.; Li, X.; Chen, R.; Fujita, H.; Lin, J. Picture fuzzy interactional partitioned Heronian mean aggregation operators: An application to MADM process. *Artif. Intell. Rev.* **2022**, *55*, 1171–1208. [[CrossRef](#)]
51. Lin, M.; Huang, C.; Chen, R.; Fujita, H.; Wang, X. Directional correlation coefficient measures for Pythagorean fuzzy sets: Their applications to medical diagnosis and cluster analysis. *Complex Intell. Syst.* **2021**, *7*, 1025–1043. [[CrossRef](#)]
52. Zhou, Q.; Wang, L.; Wu, C.; Li, H.; Du, H. Adaptive fuzzy control for nonstrict-feedback systems with input saturation and output constraint. *IEEE Trans. Syst. Man Cybern. Syst.* **2016**, *47*, 1–12. [[CrossRef](#)]
53. Zhou, X.; Cai, X.; Zhang, H.; Zhang, Z.; Jin, T.; Chen, H.; Deng, W. Multi-strategy competitive-cooperative co-evolutionary algorithm and its application. *Inf. Sci.* **2023**, *635*, 328–344. [[CrossRef](#)]
54. Zhao, T.; Chen, C.; Cao, H. Evolutionary self-organizing fuzzy system using fuzzy-classification-based social learning particle swarm optimization. *Inf. Sci.* **2022**, *606*, 92–111. [[CrossRef](#)]

55. Li, M.; Zhang, J.; Song, J.; Li, Z.; Lu, S. A Clinical-Oriented Non-Severe Depression Diagnosis Method Based on Cognitive Behavior of Emotional Conflict. *IEEE Trans. Comput. Soc. Syst.* **2022**, *10*, 131–141. [[CrossRef](#)]
56. Zhao, T.; Chen, C.; Cao, H.; Dian, S.; Xie, X. Multiobjective Optimization design of interpretable evolutionary fuzzy systems with type self-organizing learning of fuzzy sets. *IEEE Trans. Fuzzy Syst.* **2022**, *31*, 1638–1652. [[CrossRef](#)]
57. Huang, C.; Zhou, X.; Ran, X.; Liu, Y.; Deng, W.; Deng, W. Co-evolutionary competitive swarm optimizer with three-phase for large-scale complex optimization problem. *Inf. Sci.* **2023**, *619*, 2–18. [[CrossRef](#)]
58. Zhao, T.; Cao, H.; Dian, S. A self-organized method for a hierarchical fuzzy logic system based on a fuzzy autoencoder. *IEEE Trans. Fuzzy Syst.* **2022**, *30*, 5104–5115. [[CrossRef](#)]
59. Zhao, T.; Tong, W.; Mao, Y. Hybrid Non-singleton Fuzzy Strong Tracking Kalman Filtering for High Precision Photoelectric Tracking System. *IEEE Trans. Ind. Inform.* **2023**, *19*, 2395–2408. [[CrossRef](#)]
60. Rudin, K.; Ducard, G.J.; Siegwart, R.Y. Active fault-tolerant control with imperfect fault detection information: Applications to UAVs. *IEEE Trans. Aerosp. Electron. Syst.* **2019**, *56*, 2792–2805. [[CrossRef](#)]
61. Liberzon, D.; Morse, A.S. Basic problems in stability and design of switched systems. *IEEE Control Syst. Mag.* **1999**, *19*, 59–70.
62. Liu, Y.; Yan, W.; Yu, C.; Zhang, T.; Tu, H. Predefined-Time Trajectory Planning for a Dual-Arm Free-Floating Space Robot. In Proceedings of the IECON 2020 The 46th Annual Conference of the IEEE Industrial Electronics Society, Singapore, 18–21 October 2020; pp. 2798–2803.
63. Yan, W.; Liu, Y.; Lan, Q.; Zhang, T.; Tu, H. Trajectory planning and low-chattering fixed-time nonsingular terminal sliding mode control for a dual-arm free-floating space robot. *Robotica* **2022**, *40*, 625–645. [[CrossRef](#)]
64. Yao, J.; Yan, W.; Lan, Q.; Liu, Y.; Zhao, Y. Parameter Optimization of dsRNA Splicing Evolutionary Algorithm Based Fixed-Time Obstacle-Avoidance Trajectory Planning for Space Robot. *Appl. Sci.* **2021**, *11*, 8839. [[CrossRef](#)]
65. Liu, Y.; Yan, W.; Zhang, T.; Yu, C.; Tu, H. Trajectory tracking for a dual-arm free-floating space robot with a class of general nonsingular predefined-time terminal sliding mode. *IEEE Trans. Syst. Man Cybern. Syst.* **2021**, *52*, 3273–3286. [[CrossRef](#)]
66. Yan, B.; Niu, B.; Zhao, X.; Wang, H.; Chen, W.; Liu, X. Neural-network-based adaptive event-triggered asymptotically consensus tracking control for nonlinear nonstrict-feedback MASs: An improved dynamic surface approach. *IEEE Trans. Neural Netw. Learn. Syst.* **2022**. [[CrossRef](#)]
67. Van, M.; Sun, Y.; McIlvanna, S.; Nguyen, M.N.; Khyam, M.O.; Ceglarek, D. Adaptive Fuzzy Fault Tolerant Control for Robot Manipulators with Fixed-Time Convergence. *IEEE Trans. Fuzzy Syst.* **2023**. [[CrossRef](#)]
68. Ouyang, H.; Lin, Y. Adaptive fault-tolerant control and performance recovery against actuator failures with deferred actuator replacement. *IEEE Trans. Autom. Control* **2020**, *66*, 3810–3817. [[CrossRef](#)]

Disclaimer/Publisher’s Note: The statements, opinions and data contained in all publications are solely those of the individual author(s) and contributor(s) and not of MDPI and/or the editor(s). MDPI and/or the editor(s) disclaim responsibility for any injury to people or property resulting from any ideas, methods, instructions or products referred to in the content.